Geochemistry, Geophysics, Geosystems®

AGU ADVANCING EARTH AND SPACE SCIENCES

RESEARCH ARTICLE
10.1029/2023GC011063

Seismic Cycle in Bituminous Dolostones (Monte Camicia Thrust Zone, Central Apennines, Italy)

Miriana Chinello[1], Elena Bersan[1], Michele Fondriest[1], Telemaco Tesei[1], Rodrigo Gomila[1], and Giulio Di Toro[1,2]

[1]Dipartimento di Geoscienze, Università degli Studi di Padova, Padua, Italy, [2]Istituto Nazionale di Geofisica e Vulcanologia (INGV), Rome, Italy

Key Points:

- Bituminous dolostones are cut by a dense network of fractures and faults that record the main phases of the seismic cycle
- Aseismic slip occurs via cataclasis, pressure-solution, and viscous flow in bitumen while larger faults record multiple seismic ruptures
- Mirror-like surfaces are found in all faults, regardless of their displacement, and are formed during all phases of the seismic cycle

Correspondence to:
M. Chinello,
miriana.chinello@phd.unipd.it;
chinello.miri@gmail.com

Citation:
Chinello, M., Bersan, E., Fondriest, M., Tesei, T., Gomila, R., & Di Toro, G. (2023). Seismic cycle in bituminous dolostones (Monte Camicia Thrust Zone, Central Apennines, Italy). *Geochemistry, Geophysics, Geosystems*, *24*, e2023GC011063. https://doi.org/10.1029/2023GC011063

Received 30 MAY 2023
Accepted 26 OCT 2023

Author Contributions:
Conceptualization: Miriana Chinello, Michele Fondriest, Telemaco Tesei, Giulio Di Toro
Data curation: Miriana Chinello, Elena Bersan, Michele Fondriest
Funding acquisition: Giulio Di Toro
Investigation: Miriana Chinello, Elena Bersan, Michele Fondriest, Telemaco Tesei, Rodrigo Gomila, Giulio Di Toro
Methodology: Michele Fondriest, Rodrigo Gomila, Giulio Di Toro
Project Administration: Giulio Di Toro
Supervision: Michele Fondriest, Giulio Di Toro

Abstract Seismic ruptures often propagate along fault zones cutting km-thick sequences of carbonates (e.g., Wenchuan M_w 7.8, 2008, China; L'Aquila M_w 6.1, 2009, Italy). As a consequence, fault rock assemblages may record the seismic cycle under a wide range of loading conditions, temperatures (>1,000°C during co-seismic slip), and fluid-rock interactions. The Monte Camicia Thrust Zone in the Italian Central Apennines is exhumed from ~3 km depth. We studied the seismic cycle recorded by a network of faults cutting bituminous dolostones in the footwall of the Monte Camicia Thrust. These faults accommodate up to several meters of displacement. Slip zones are mm- to cm-thick and bounded by ultra-polished ("mirror-like") surfaces independently of their displacement. At the microscale, deformation is accommodated by cataclasis and pressure-solution in carbonates, and viscous flow in the foliated bitumen. Some of the faults with displacements >0.10 m have multiple slip zones, separated by "mirror-like" surfaces, and include clasts of foliated bitumen and fragments of older slip zones sealed by calcite precipitation. We conclude that (a) slip zones record post- to inter-seismic (foliated bitumen) and co-seismic (fragments of bitumen) deformation in a fluid-rich environment (calcite precipitation) and (b) mirror-like surfaces formed during all phases of the seismic cycle.

Plain Language Summary Earthquakes originate and propagate along faults and release elastic strain energy stored in their wall rocks for centuries to millennia in a matter of seconds. Consequently, earthquakes represent the paroxysmal phase of the seismic cycle, which includes pre-, co-, post-, and inter-seismic phases. Most deformation mechanisms occurring in fault zones during the seismic cycle are transparent to seismological and other geophysical investigations. Instead, ancient fault zones exposed at the Earth's surface allow us to investigate the deformation mechanisms activated during the seismic cycle. These mechanisms operate under varying conditions of temperature, stress, fluid-rock interaction and slip rate (relative motion of the fault wall rocks $>10^{-4}$ m/s during co-seismic slip and from 0 to $\approx 10^{-7}$ m/s in the other phases). We studied a network of faults that cut through bituminous dolostones in the Italian Central Apennines. These faults are characterized by the presence of light-reflecting (mirror-like) surfaces. We found that the slip zones beneath the mirror-like surfaces (MSs) recorded deformation mechanisms associated with the four phases of the seismic cycle. Furthermore, MSs, whose mechanism of formation is debated in the literature, may form during all phases of the seismic cycle.

1. Introduction

In the upper crust, seismic ruptures associated with mainshocks and aftershocks often propagate along fault zones, cutting km-thick sequences of carbonates. Examples of these earthquakes include those occurring in the Italian Apennines (Irpinia 1980, M_w 6.9; L'Aquila 2009, M_w = 6.1; Amatrice-Norcia 2016, M_w = 6.0 and M_w = 6.5; Cocco et al., 1999; Chiarabba et al., 2009; Chiaraluce, 2012; Improta et al., 2019; Valoroso et al., 2013; Figure 1a) and Southern Alps (e.g., Friuli 1976, M_w = 6.5; Finetti et al., 1979), the Balkans (Gulf of Corinth 1981, M_w = 6.7, 6.4, 6.3; Albania 2019, M_w = 6.4; Govorčin et al., 2020; Papadopoulos et al., 2020; Won-Young et al., 1984), and the Longmenshan belt (Wenchuan 2008, M_w = 7.8; Toda et al., 2008). High-resolution geodetic, geophysical, and seismological studies yield a wealth of information about the source properties and characteristics of the mainshock ruptures, and on the architecture of the fault networks associated with these seismic sequences (Baccheschi et al., 2019; Chiaraluce et al., 2011, 2017; Cirella et al., 2009; Collettini et al., 2022; Pizzi et al., 2017; Scognamiglio et al., 2018; Valoroso et al., 2014). These studies also yield constraints on the ambient conditions of seismic faulting at depth. However, the

Visualization: Miriana Chinello, Elena Bersan, Rodrigo Gomila
Writing – original draft: Miriana Chinello
Writing – review & editing: Miriana Chinello, Elena Bersan, Michele Fondriest, Telemaco Tesei, Rodrigo Gomila, Giulio Di Toro

detailed architecture of fault zones and the type of deformation mechanisms active during the seismic cycle are currently transparent to these investigation techniques. Field studies of fault zones exposed at the Earth's surface coupled with microstructural, mineralogical, geochemical and rock deformation experimental investigations attempt to constrain the deformation mechanisms activated throughout the seismic cycle (e.g., Balsamo et al., 2014; Collettini et al., 2013; Cox, 1995; De Paola et al., 2015; Delle Piane et al., 2017; Di Toro et al., 2012; Fondriest et al., 2013; Gratier et al., 2002, 2023; Parry & Bruhn, 1990; Sibson, 1992; Smeraglia et al., 2022; Smith et al., 2011, 2013; Tesei et al., 2014). These studies reveal that, in massive carbonate fault zones, deformation is localized in continuous sub-mm to few cm-thick slip zones within tens of cm- to m-thick fault cores, composed of cataclastic rocks that accommodate most of the shear strain (Agosta & Aydin, 2006; Demurtas et al., 2016; Fondriest et al., 2020; Jackson & McKenzie, 1999; Smith et al., 2011). The fault cores are embedded in m- to km-thick damage zones where deformation is accommodated by minor faults, fractures, folds, and veins (Caine et al., 1996; Demurtas et al., 2016; Faulkner et al., 2010; Fondriest et al., 2015, 2020; Wibberley et al., 2008). In damage zones, the density of fault/fracture decays, often discontinuously, from the fault core toward the host rocks (Agosta & Kirschner, 2003; Billi et al., 2003; Kim et al., 2004; Sibson, 1977).

The seismic cycle includes four main phases: pre-seismic, co-seismic, post-seismic, and inter-seismic (Scholz, 2019). During the inter-seismic phase, fault zone rocks are in almost static contact, whereas during the pre-seismic, co-seismic and post-seismic phases the fault zones host ruptures propagating from <nm/s (e.g., sub-critical cracks in the pre-, post- and inter-seismic, Atkinson & Meredith, 1987) to km/s (co-seismic) and faults slip from aseismic (0 to $\approx 10^{-7}$ m/s: pre-, post-seismic) to seismic ($>10^{-4}$ m/s: co-seismic) slip rates (Cowan, 1999; Rowe & Griffith, 2015). This large range of loading and slip conditions plus the frequent presence of pressurized fluids (H_2O, CO_2, hydrocarbons, etc.) results in the formation of several fault zone rock types and structural features including breccias, cataclasites, in situ shattered rocks, fault-veins, "fluidized" cataclasites/gouges, polished to ultra-polished (nm-scale roughness) fault surfaces (or Mirror-like Surfaces, MSs), etc. (Collettini et al., 2014; Demurtas et al., 2016; Fondriest et al., 2012, 2013, 2015; Jackson & McKenzie, 1999; Leah et al., 2018; Masoch et al., 2019; Ohl et al., 2020; Siman-Tov et al., 2013; Smith et al., 2011). The dominant deformation mechanisms documented in carbonate-built fault rocks are cataclasis, pressure-solution and precipitation, low-temperature crystal plasticity and twinning (Delle Piane et al., 2017; Hadizadeh, 1994; Kennedy & White, 2001; Koopman, 1983; and references therein). In addition, during the co-seismic phase, other temperature-activated phenomena could be activated. Due to high temperatures achieved in the slip zone during co-seismic slip (up to 1,250°C; Aretusini et al., 2021; Billi & Di Toro, 2008), deformation mechanisms may include cataclasis, grain size- and temperature-dependent plasticity associated with decarbonation (and possibly graphitization) of calcite and dolomite plus deformation processes such as thermal fluid pressurization and gouge fluidization (Collettini et al., 2013; De Paola et al., 2015; Fondriest et al., 2013; Pozzi et al., 2019; Smith et al., 2011, 2013; Spagnuolo et al., 2015). Some structures such as MSs, possibly form in different phases of the seismic cycle in carbonate-built fault zones. In fact, experimental MSs have been obtained by shearing gouges and solid specimens of limestone and dolostone at co-seismic (>0.1 m/s; Boneh et al., 2013; Chen et al., 2013; Fondriest et al., 2013; Siman-Tov et al., 2015; Smith et al., 2013; Pozzi et al., 2018), but also at sub-seismic slip rates (≈0.1–10 μm/s; Passelègue et al., 2019; Tesei et al., 2017; Verberne et al., 2014). Thus, MSs can be the result of a morphological convergence of slow (i.e., aseismic) and fast (co-seismic) deformation mechanisms and processes.

Here we discuss original field data and microstructural observations of faults cutting the footwall rocks (bituminous dolostones) of the Monte Camicia Thrust located in the Gran Sasso Massif (Central Apennines, Italy). We propose that microstructures of the fault cores (often bounded by MSs) record a polyphasic deformation history that may belong to the different phases of the seismic cycle. The studied (often multiple) slip surfaces and slip zones are associated with pre- and post-seismic phases (cataclasis, smearing and viscous flow of bitumen, pressure-solution), co-seismic slip (bitumen embrittlement and fragmentation) and inter-seismic fault strength recovery. Furthermore, several MSs are also found in faults/fractures accommodating negligible displacements (<1 mm), supporting the hypothesis that these surfaces may be the result of rock fracturing followed by static fluid-rock interaction. In addition to that, the new field data clarify the local relationship between compressive and extensional structures in the area, supporting the interpretation of the reverse kinematics of the Monte Camicia Thrust followed by minor and localized normal fault reactivation (Lucca et al., 2019).

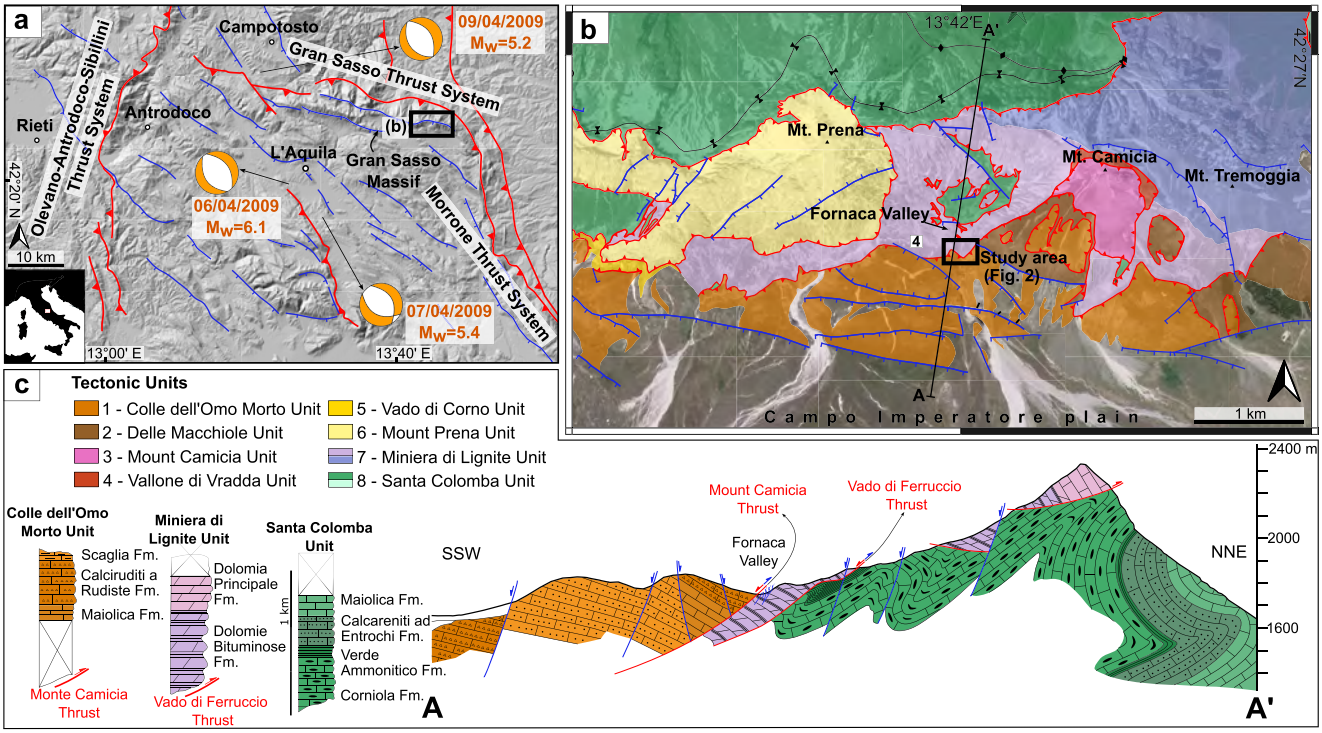

Figure 1. Geological setting of the Campo Imperatore area (Central Italy). Main thrust faults are in red, normal faults in blue and folds in black. (a) Map showing the main faults of the northern portion of the Central Apennines. The focal mechanisms refer to the mainshocks of the L'Aquila 2009 seismic sequence (modified after Pizzi et al., 2017). (b) Structural map of the Monte Camicia area (modified after Ghisetti & Vezzani, 1986b; Lucca et al., 2019). Colors refer to the tectonic units (see panel c) defined by Ghisetti and Vezzani (1986b). The black inset shows the location of the study area. (c) Cross-section A-A' (see panel b), stratigraphy and tectonic units.

2. Geological Setting

2.1. Gran Sasso Massif

The Gran Sasso Massif (2,912 m a.s.l.) is the highest relief of the Apennine fold-and-thrust belt. The massif is delimited to the north by the Gran Sasso Thrust System (GSTS), which is bounded by the Olevano-Antrodoco-Sibillini Thrust System to the west and linked to the Morrone Thrust System to the east (Ghisetti, 1987; Figure 1a). The GSTS is an arcuate thrust front with northward vergence. The western segment trends WNW-ESE and accommodates almost pure N-S compression, while the eastern N-S trending segment accommodates dextral strike-slip along thrust faults (Cardello & Doglioni, 2015; Ghisetti, 1987; Ghisetti & Vezzani, 1991; Speranza et al., 2003; Vezzani et al., 2010; Figure 1a). In particular, the GSTS is composed of imbricate thrust sheets including Upper Triassic-Lower Cenozoic carbonates scraped from the sedimentary cover of the westerly subducting Adriatic plate (Ghisetti & Vezzani, 1991). The thrust sheets are bounded by eight N-verging thrust faults (ϕ1–ϕ8 from top to bottom) developed from the Messinian to early middle Pliocene (Ghisetti, 1987; Ghisetti & Vezzani, 1991; Figures 1b and 1c). The thrust faults mainly strike WNW-ESE, dip 15°–30° to SSW and are often arranged in an out-of-sequence geometry (Ghisetti & Vezzani, 1991; Speranza et al., 2003; Vezzani et al., 2010).

Since late Messinian, the GSTS was subjected to extensional gravitational collapse coaxial with the north-eastward compression, probably due to gravity-induced re-equilibration of the GSTS (Lucca et al., 2019). The GSTS was then dissected by E-W and WNW-ESE trending normal faults with evidence of Quaternary deformation and surface ruptures (since Late Pleistocene-Holocene; Galadini & Galli, 2000; Figure 1a). Stratigraphy and inherited synsedimentary Jurassic normal faults are responsible for spatial heterogeneities in both the compressional and extensional deformation stages (Cardello & Doglioni, 2015) with documented reactivation of Jurassic faults during the Quaternary extension (Centamore et al., 2002).

The study area is a gully located in the Fornaca Valley (Gran Sasso Massif, Figure 1b) between Monte Prena and Monte Camicia along the northern margin of the Campo Imperatore plain (42°25′48.7″N, 13°42′00″; Figure 1b).

2.2. Stratigraphy

In the Fornaca Valley are exposed rocks located at the transition between a Late Triassic-Early Jurassic carbonate platform (W-part) and an euxinic to open pelagic basin (E-part) (Adamoli et al., 1984, 1990; Barchi & Bigozzi, 1995).

The bituminous dolostones (i.e., *Dolomie Bituminose* Fm. *auct.*) outcrop in the Fornaca Valley has a thickness up to 180 m (Figure 1c), while the true thickness is unknown due to intense tectonization (Adamoli et al., 1990; Bertinelli et al., 2004). The beds are made of thin layers (mm to tens of cm) of gray and black (organic matter-rich) dolomites, alternated to dolostone beds up to 10 m thick organized in coarsening and thickening upwards cycles (Adamoli et al., 1984; Barchi & Bigozzi, 1995). Convolute laminations, synsedimentary micro-faults and mega-breccia bodies (olistoliths up to decametric in size) of dolostones, the latter supplied from the platform edge, are related to sediment compaction, fluid expulsion and gravitational movements (Adamoli et al., 1990; Bertinelli et al., 2004). The depositional environment corresponds to an upper carbonate platform slope to a tidal flat with multiple anoxic episodes (Adamoli et al., 1984). The upper part of the *Dolomie Bituminose* Fm. contains chert nodules, testifying a deepening of the basin and a possible link to the open sea (Adamoli et al., 1984). The TOC (Total Organic Carbon) content of *Dolomie Bituminose* Fm. is up to 40% (Katz et al., 2000) and Apatite Fission Track and Vitrinite Reflectance analyses define this as an immature source rock that experienced a maximum temperature of 100°C during burial (Rusciadelli et al., 2005).

In the area outcrops also the Middle Jurassic *Corniola* limestones (i.e., *Corniola* Fm.; Figure 1c), composed of micritic cherty limestones, typical of distal platform scarps and proximal basins, organized in 50–100 cm-thick beds with intercalation of detrital horizons (e.g., turbidites) made of grainstones and packstones. The basal part can be locally dolomitized, and the maximum thickness of this formation is about 500–600 m (Adamoli et al., 2012; Ghisetti & Vezzani, 1986b).

Rudist calcarenites (i.e., *Calciruditi a Rudiste* Fm.) is a 60–350 m thick Upper Cretaceous-Eocene unit (i.e., *Calcareniti e Calciruditi a Fucoidi* Fm. in Adamoli et al., 2012), stratigraphically comprised between the *Maiolica* Fm. and *Scaglia* Fm. (Figure 1c; Adamoli et al., 2012; Ghisetti, 1987). The rudist calcarenites are made of 2–5 m-thick beds of whitish calcarenites and calcirudites, with abundant rudist fragments interbedded with oolithic limestones (Ghisetti & Vezzani, 1986b). This formation is related to a slope environment (Adamoli et al., 2012).

2.3. Monte Camicia Thrust

At the bottom of the Fornaca valley two faults of the GSTS are outcropping, the Vado di Ferruccio Thrust ("ϕ7" in Ghisetti, 1987; "Upper Thrust" in D'Agostino et al., 1998) and the Monte Camicia Thrust ("ϕ1/T1" to "ϕ2/T2" in Ghisetti, 1987; Ghisetti & Vezzani, 1986b; Leah et al., 2018; Pace et al., 2014), bounding a tectonic sliver of Upper Triassic bituminous dolostones (Figures 1b and 1c). The Vado di Ferruccio Thrust dips 11°–50° to the S-SW (Leah et al., 2018) and places the bituminous dolostones of the hanging wall on *Corniola* limestones of the footwall. The Monte Camicia Thrust dips at an average of 33° to the south and places Cretaceous rudist calcarenites of the hangingwall onto Upper Triassic bituminous dolostones of the footwall (Figures 1c, 2, and 3a; Lucca et al., 2019). Because of the younger-on-older contact typical of normal faults, various hypotheses were proposed regarding the kinematics of the Monte Camicia Thrust:

1. Out-of-sequence thrust fault. This hypothesis is supported by the presence of Riedel-type secondary faults, fault-related veins and stylolites networks whose attitude and sense of shear are consistent with the transport of the thrust sheet from the southern backlimb onto the northern forelimb of the Gran Sasso anticline (Ghisetti and Vezzani, 1991, 1997; Vezzani et al., 2010);
2. Synsedimentary Mesozoic steeply dipping normal fault rotated to lower dip angle during the Neogene thrust-related folding. This hypothesis is supported by structural data (i.e., drag folds, synthetic R-type Riedel shear planes, cut-off angle relations), stratigraphic constraints and balanced geological cross sections (Calamita et al., 2002, 2004; Pace et al., 2014; Tozer et al., 2002);
3. Low angle normal fault which reactivates late Messinian-middle Pliocene thrusts. This hypothesis is supported by structural analysis and field mapping together with simple geometrical and flexural elastic models (D'Agostino et al., 1998);
4. Out-of-sequence thrust reactivated as a normal fault (this hypothesis reconciles the hypothesis 1 and 3). The Monte Camicia Thrust formed as an out-of-sequence thrust in a subaerial environment and then was reactivated in extension, due to footwall collapse coeval with the development of the Campo Imperatore

10.1029/2023GC011063

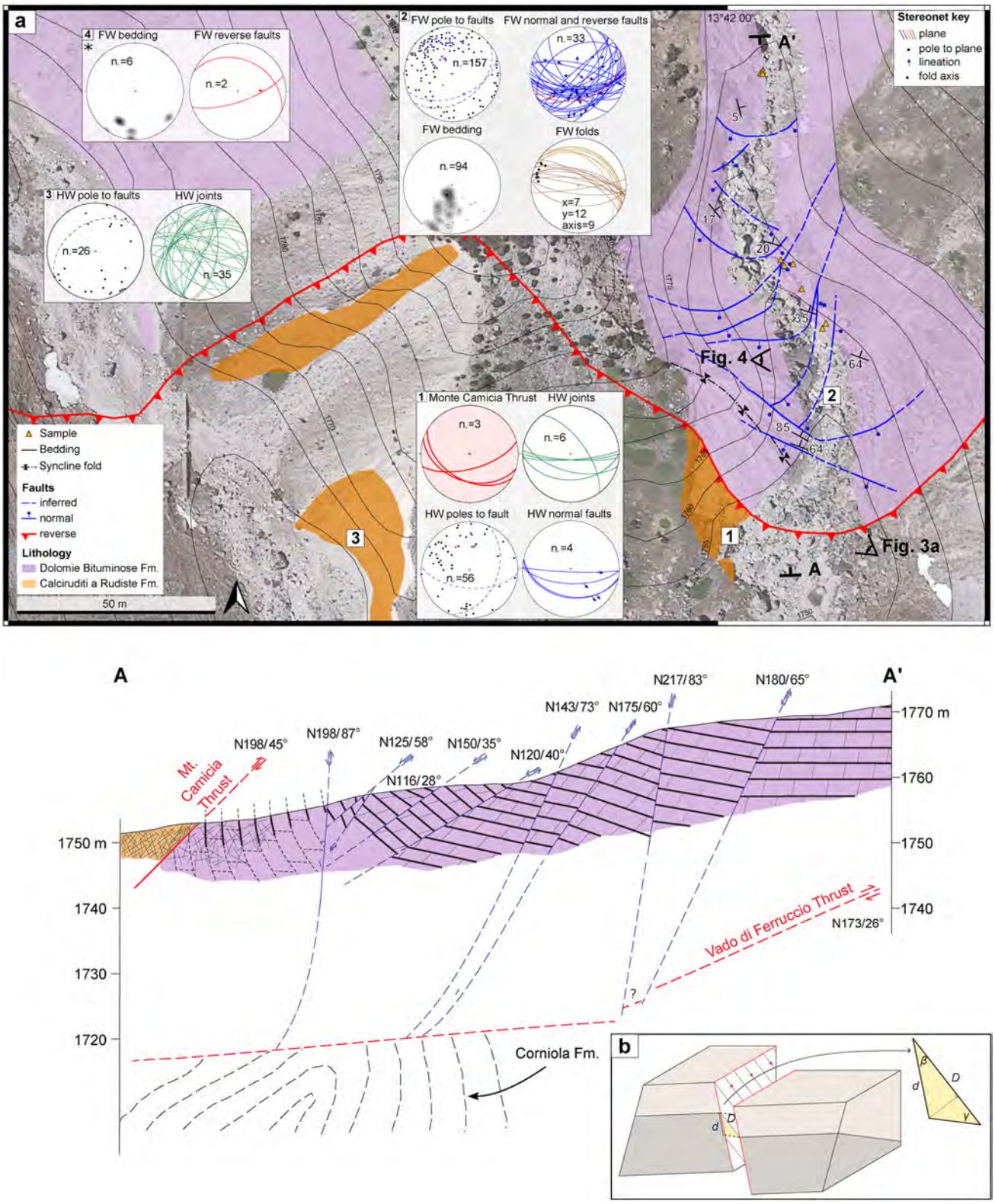

Figure 2.

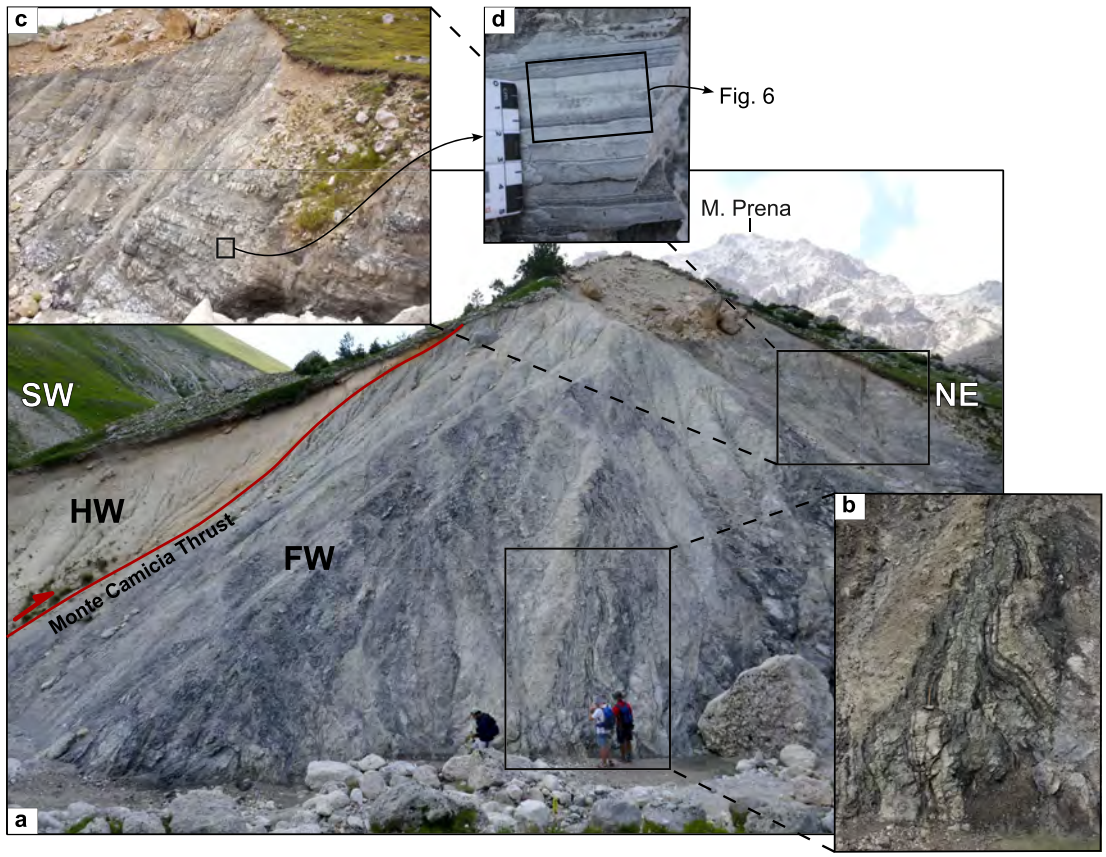

Figure 3. Monte Camicia Thrust Zone in the surveyed gully. (a) Monte Camicia Thrust exposure. Folded sub-vertical strata of the *Dolomie Bituminose* Fm. in the footwall (FW) and highly damaged strata of *Calciruditi a Rudiste* Fm. in the hangingwall (HW). (b) and (c) Sub-vertical (b) and sub-horizontal (c) strata of the bituminous dolostones in the footwall at about 10 and 50 m from the main fault of the thrust. (d) Undeformed bituminous dolostones showing the color layering due to different content in organic matter and the polarity of the strata.

(subaerial) extensional fault system during Quaternary (Lucca et al., 2019). This hypothesis is based on structural plus isotopic data, and further supported by evidence presented in this study.

The outcrops chosen for this study are located in an N-S oriented gully about 150 m long in the Fornaca Valley (Figures 1b and 1c). Here WNW-ESE and NW-SE trending normal faults with MSs cut the bituminous dolostones and are related to the Quaternary extension that dissected the GSTS.

3. Methods

3.1. Fieldwork and Sample Preparation

Field-geology surveys at 1:1,000 were conducted using orthorectified aerial photographs (spatial resolution 0.20 m/pix, courtesy of the Regione Abruzzo: opendata.regione.abruzzo.it) as mapping bases. Structural data of faults, fractures, folds and bedding were collected in four locations and digitized using QGIS© 3.10 and Stereonet 11 (Allmendinger et al., 2012; Cardozo & Allmendinger, 2013). Fault separation (*d*) and attitude of outcrop surfaces were also measured for not dip-slip faults to compute the displacement (*D*) using the following equation:

Figure 2. Structural data collected in the surveyed area. (a) Map and geological cross section (A-A'). Monte Camicia Thrust and reverse faults are in red; normal faults are in blue. The stereoplots (lower hemisphere projection) summarize the structural data (faults, bedding, joints and folds) collected in four localities (Stop 1–4; numbers in white boxes; location of structural stop n. 4 is in Figure 1b) in the hangingwall (HW) and in the footwall (FW). In the stereoplots, the contours of the poles to bedding are in black, poles to faults with uncertain kinematics and planes are in black, poles to normal faults and planes are in blue, poles to reverse faults and planes are in red; joint surfaces are in green and fold limbs are in dark yellow and brown. Dashed lines represent mean fault surfaces (blue for normal faults and black for faults with uncertain kinematics). Arrows represent fault *striae* and point toward the direction of movement of the hangingwall. Diamonds represent fold axis. The stereoplot with a light red background refers to the structural data of the Monte Camicia Thrust. (b) Sketch showing how fault displacement was computed from fault separation and attitude of fault, outcrop surface, and bedding.

$$D = d \times [\sin \beta \times \cot \gamma + \cos \beta]$$

where β is the angle between fault lineation and the intersection fault surface—outcrop surface, and γ is the angle between the fault lineation and the intersection bedding—fault surface (Figure 2b).

Around 60 samples of fault and host rocks were collected both in the footwall and the hangingwall of the Monte Camicia Thrust. Nine samples were consolidated and prepared in cm-in-size rock chips or polished "thin" sections (3 mm and 30 μm thick respectively) cut perpendicular to the fault surface and parallel to striations for optical and Scanning Electron Microscope (SEM) microstructural observations. For the SEM observations, the samples were coated with a ca. 10 nm thick carbon film. Sample preparation was conducted at the Department of Geosciences of the University of Padua.

3.2. Microstructural Analyses

Transmitted-light optical microscopy was used to recognize specific microstructural features at the thin section scale while detailed microstructural analyses were then performed with two Field-Emission Scanning Electron Microscopes:

- JEOL JSM-6500F FE-SEM installed at the High Pressure-High Temperature Laboratory of the Istituto Nazionale di Geofisica e Vulcanologia in Rome (INGV);
- TESCAN SOLARIS dual beam FIB-FE-SEM installed at the Department of Geosciences at the University of Padua.

Operational conditions of the electron beams were 10–15 keV with ~6–10 mm as working distance for the analysis scan mode; 5–7 keV and 3–4 mm as working distance for the ultra-high resolution scan mode in University of Padua. We performed Back-Scattered Electron across the principal slip zones and Secondary Electron (SE) imaging of the MSs.

4. Monte Camicia Thrust Zone

In the southernmost part of the studied gully, the Monte Camicia Thrust (Figures 1c, 2a, and 3a) strikes on average E-W to WNW-ESE and is characterized by a sharp principal fault surface that dips between 40° and 50° to the south (Stop 1 in Figure 2a) as measured by Lucca et al. (2019) in the south-eastern side of the gully (see structural site CF15 in Lucca et al., 2019).

The hangingwall of the Monte Camicia Thrust (Figures 2a and 3a) consists of several tens of meters thick shattered rudist calcarenites (pertaining to the *Calciruditi a Rudiste* Fm.) with fractures spaced less than 1–2 cm, and cut by minor faults striking E-W and NNE-SSW and dipping 40°–80° mainly toward ESE-SSE (i.e., parallel to oblique to the Monte Camicia Thrust) and few others toward N and NW, in proximity to the principal fault surface (Stops 1 and 3 in Figure 2a). Faults with normal kinematics dip 40°–90° toward the S (i.e., sub-parallel to the Monte Camicia Thrust) with transtensional sinistral shear (Stop 1 in Figure 2a). On top of the principal fault surface (Stop 1 in Figure 2a), joints dip mainly toward the S, while their attitude is more scattered moving to the west (Stop 3 in Figure 2a).

The footwall block of the Monte Camicia Thrust includes dm- to m-thick strata of folded and faulted bituminous dolostones (pertaining to the *Dolomie Bituminose* Fm.) (Figure 3a). A gray color gradation across individual strata reflects the percentage of organic matter, which decreases from the base (dark gray/black) to the top (light gray; Figure 3d) of the stratum, probably due to variation of oxygen content in the euxinic basin during sedimentation. The strata dip toward N and NE; on average, their dip angle gradually decreases from 65° to 88° near the main fault surface to ~5°–10° at 50–60 m north of the Monte Camicia Thrust (Stop 2 in Figure 2a; Figures 3b and 3c). Similar sub-vertical attitudes of the strata were measured to the west of the study area (see stop 4 in Figure 1a and stereoplot in Figure 2a). Along the east side of the gully the heavily faulted dolomitic beds form a m-scale open asymmetric fold (interlimb angle >100°) with axes plunging WNW (Figure 4a); in the same area, minor asymmetric folds (Stop 2 in Figure 2a; Figures 4b and 4c) are characterized by longer limbs dipping at high angle (>70°) and the shorter ones dip at relatively low angle (20°–40°) both toward the north in a *Z*-type fashion (Ramsay & Huber, 1987), with axes gently plunging 5°–10° toward WNW (i.e., sub-parallel to the strike of the Monte Camicia Thrust). The polarity of the beds, inferred from the distribution of organic matter, together

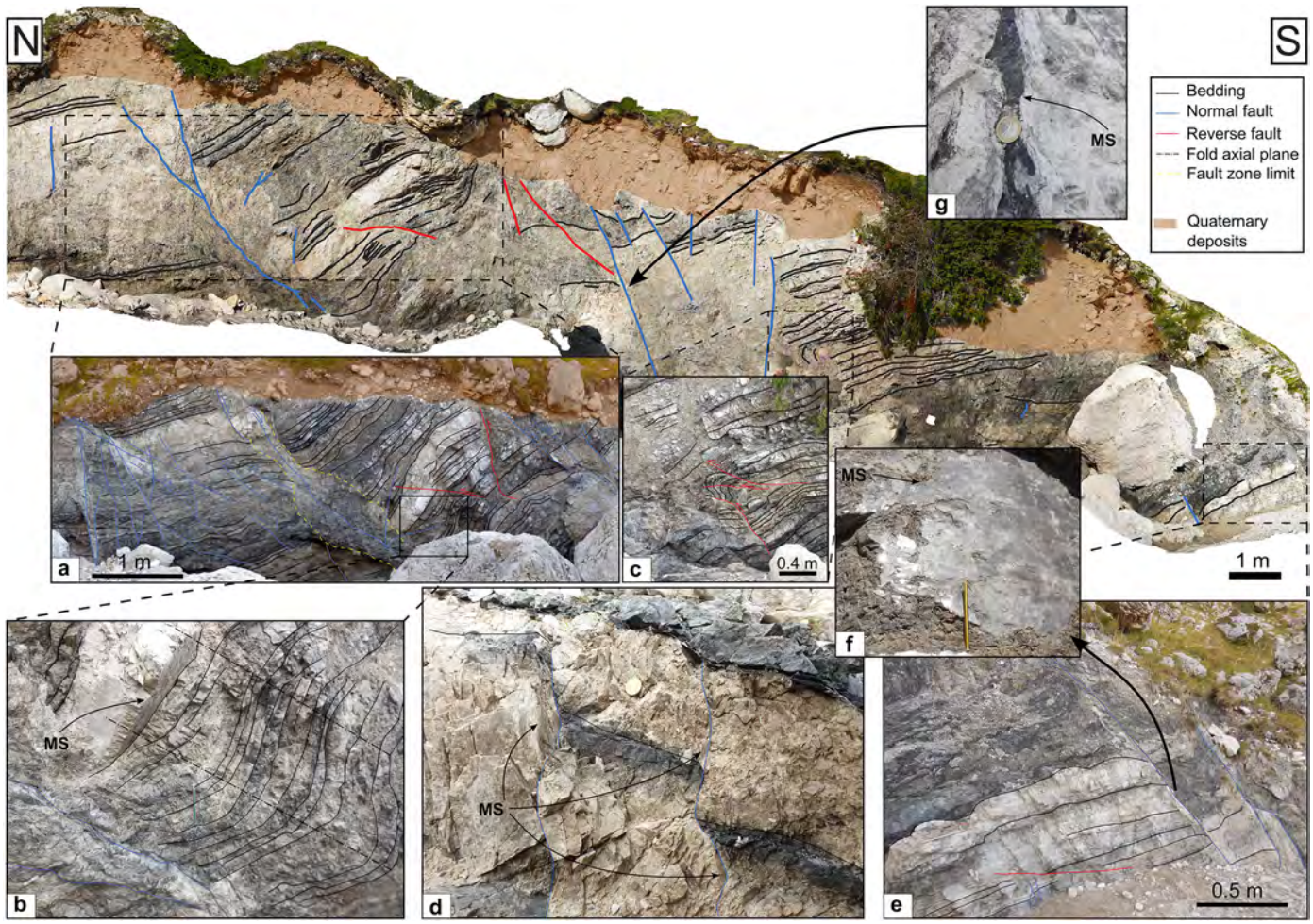

Figure 4. Main structural features in the bituminous dolostones at the footwall of the Monte Camicia Thrust (photomosaic of the east side of the surveyed gully). (a) Low and high angle normal faults cross-cutting both each other and folded strata. (b, c) *Z*-type asymmetric parasitic folds (longer limbs dipping at high angle) sometimes developed on strata with a mirror-like surface (MS) along the bedding interface (b). (d) Small displacement (<8 cm of slip) normal faults with MSs. (e) High angle normal faults with more than 1 m of slip displacement. (f) MS in (e). (g) MS with smeared bitumen (black).

with the attitude of the strata and the presence of asymmetric folds suggest that the bituminous dolostones were dragged to form a decametric-scale synform fold with the axis striking ca. E-W in the footwall of the Monte Camicia Thrust (Figure 2a). The footwall of the Monte Camicia Thrust is cut by a dense network of minor faults mostly striking WSW-ENE and dipping 85°–50° toward S and SE, and accommodating normal dip-slip to transtensional sinistral shear displacement (Figure 2a). Few transpressive faults and back-thrusts dipping 30° and 50°–70° toward NNE and SSE respectively are also present (Stop 2 in Figure 2a). Low to high angle normal faults crosscut each other (Figures 4a and 4e); these cross-cutting relations and the separation of the strata along the faults allowed us to estimate fault displacements up to 11 m. The most relevant structural features described above are shown in the geological map of the southernmost part of the Fornaca valley and in the N-S cross section (Figure 2a).

5. Faults and Fractures Cutting the Bituminous Dolostones

5.1. Field Observations

In the bituminous dolostones, minor faults have cataclastic (i.e., cohesive) slip zones whose thickness, generally increases with the displacement, from invisible to the naked eye to few cm. The slip zones are composed of dolostone fragments and, to a less extent, bitumen immersed in a calcite- and/or bitumen-rich matrix. The slip zones are usually bounded by MSs independently of the fault displacement (Figures 4d, 4f, and 4g). MSs are also

	SAMPLE	DIP AZIMUTH	DIP ANGLE	PITCH	DISPLACEMENT (m)	NOTE
1	2021-FTW-02	146	77	80NE	3.83	MS on dolostone; two MSs (FW and HW)
2	2021-FTW-08b	0-50	90	90	< 0.001 m	wavy surface; two MSs (FW and HW) on bitumen
3	2021-FTW-08c	3	15	-	0.05	MS on dolostone and bitumen
4	2021-FTW-08e	3	20	90	0.025	MS on dolostone
5	2019-CT-07	150	75	90	0.12	no preserved striae in the collected sample; two MSs (FW and HW)
6	2019-CT-10	10	65	-	-	folded bedding (limb)
7	2019-CT-12	125	45	57E	11.22	MS on bitumen
8	2017-CAM-01	96	55	76N	0.87	MS on bitumen
9	2017-CAM-05	180	41	62W	1.23	MS on bitumen

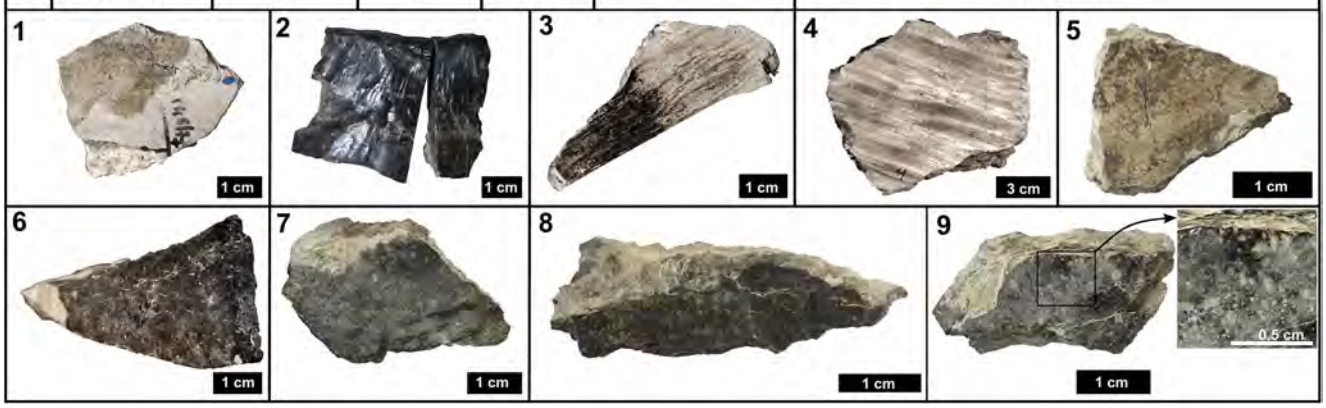

Figure 5. Summary table and photos of the studied samples.

found at the interface between the folded and unfolded strata (Figure 4b). The MSs reflect incident light, have a porcelain-like appearance, and range from light brown color (when they cut pure dolomitic beds) to dark gray or blackish (when they cut bitumen rich layers). The blackish color of the MS can be attributed to the smearing of bitumen, which contains "truncated" dolostone clasts (zoom of sample 9 in Figure 5). Fault *striae* are not always recognizable in all the samples despite the mirror-like appearance (Figure 5). About 60 samples of MSs and related slip zones were collected from normal faults with different dip, dip azimuth and cumulative displacement for microstructural analyses.

5.2. Microstructural Observations

Two host-rock and nine representative fault rock samples were selected for microstructural analysis from faults with displacement ranging from <1 mm to 11.2 m (Figure 5).

5.2.1. Host Rock

Far from the faults, the host bituminous dolostones consist of a foliated rock (parallel to the bedding) made of an alternation of cm-thick layers with higher content of dolomitic grain aggregates (tens of μm in size), and mm-thick layers with higher content in organic matter (Figure 6a). The latter layers include primary organic matter (i.e., "macerals," recognized at the optical microscope) belonging to the groups of Kerogen type I and II (Mastalerz et al., 2018), pre-oil solid bitumen, framboidal pyrite, clay minerals and euhedral calcite crystals (Figure 6). Pre-oil solid bitumen appears as a dark uniform material that fills both pores and inter- to intra-fractures in the dolomite aggregates (Mastalerz et al., 2018; Figures 6b and 6c). Macerals (alginite) and clay minerals have a preferential shape orientation and sometimes wrap dolomite or calcite clasts with a porphyroclastic-like shape (Figure 6b).

5.2.2. Fault Slip Zones and Associated Mirror Surfaces

All the selected normal fault samples include MSs, independent of their displacement. Usually, the slip zones cut intensely deformed dolostones, microbreccia and proto-cataclasites (Figures 7a–7c and 7f) or less deformed dolostones (Figures 7d and 7e) sometimes affected by bitumen-rich stylolites with the orientation of the foliation

10.1029/2023GC011063

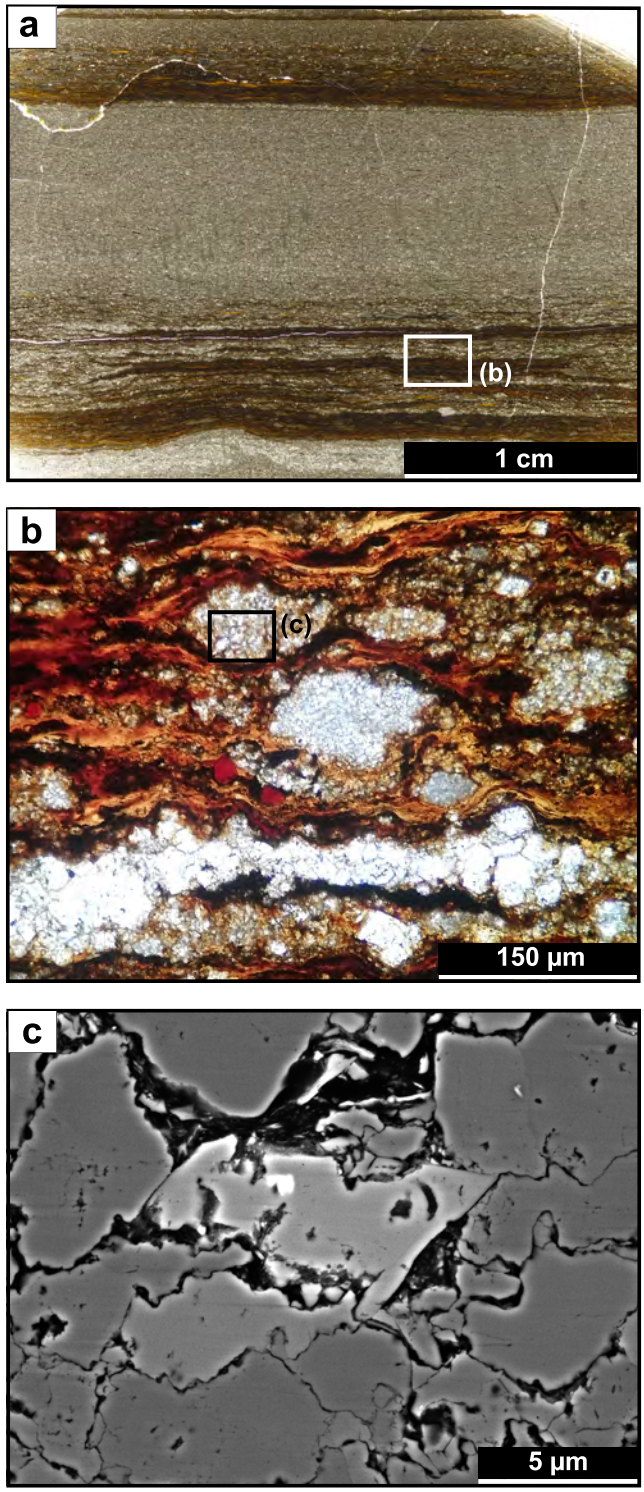

Figure 6. Typical facies of the host rock bituminous dolostones. (a) Bituminous dolostones with characteristic foliation (parallel Nicols, optical microscope image). (b) Organic matter-rich layer. Several macerals (i.e., primary organic matter) are recognizable, including alginite (orange in color elongated algal bodies) and resinite (red oval in shape bodies). Solid bitumen is the black matter filling the voids and boundaries between the clasts. Aggregates of dolomite grains are whitish in color (see panel (a) for location, parallel Nicols, optical microscope image). (c) Dolomite grains (dark gray in color) and sub-idiomorph calcite grains affected by the pressure-dissolution process (see panel (b) for location, SEM-BSE image).

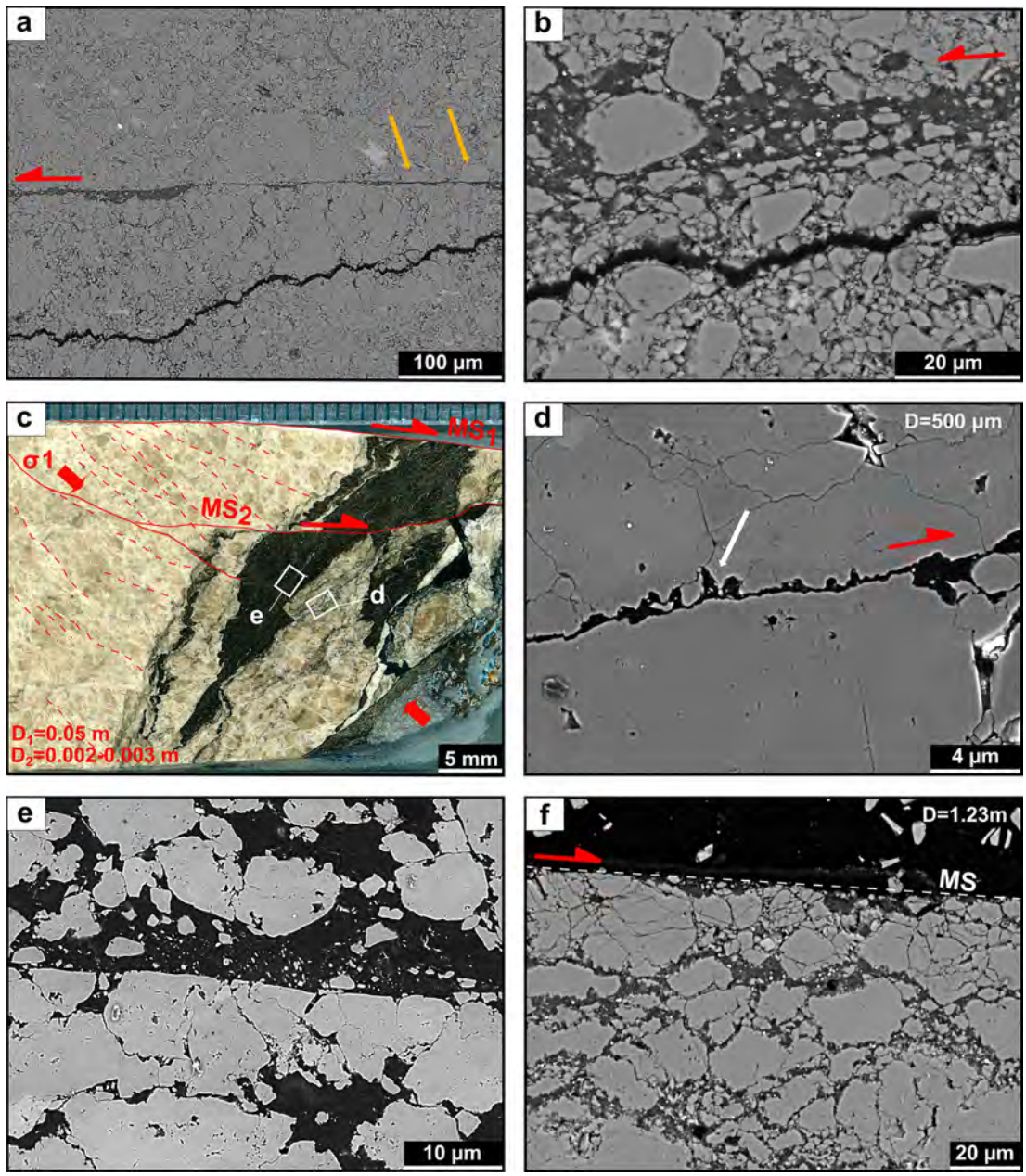

Figure 7. Microstructures of slip zones collected from normal faults with displacement from less than 1 mm up to 1.23 m. (a) and (b) Slip zone (secondary fault in sample 5) filled by bitumen (dark gray in color) bounded by truncated dolostone clasts (yellow arrows). Dolostone clasts in the bituminous-rich slip zone are preferentially oriented with the long axis sub-parallel to the wall rocks. (c) Slip and damage zone beneath a mirror surface (sample 3). A minor fault with a mirror-like appearance accommodated 2–3 mm of slip ("MS_2"; fractures are marked with dashed red lines; thick red arrows show the inferred orientation of the maximum principal stress, σ_1). (d) Minor fault decorated by bitumen (sample 3) with about 500 µm of slip. Dissolution of dolostone grains in the wall rock (formation of the stylolitic-like wall rock-bitumen contact (white arrow) is aided by the presence of bitumen. (e) Sharp contact between dolostone and bitumen (sample 3). Dolostone clasts are embedded in a bitumen-rich layer visible in (c). (f) Slip zone beneath a mirror surface (sample 9, 1.23 m of slip) with dolostone grains with sutured grain boundaries and indented grains immersed in a bitumen-rich matrix. All SEM-BSE images except for (c) (parallel Nicols optical scan of the thin section). D = displacement. Red arrow = shear sense.

perpendicular to the maximum shortening direction (tectonically induced foliation; Figure 7c). Small (<1 cm) displacement faults include a single slip zone composed of patches of continuous <20 µm-thick layer of smeared bitumen that contains ultra-fine dolostone grains (from hundreds of nm to few µm in size; Figures 7a, 7b, 7d, and 7e). The elongated grains are aligned and oriented with their long axis parallel to the fault surface (Figure 7b). At higher displacement (123 cm) the slip zone consists of <200 µm-thick dolostone ultracataclasite

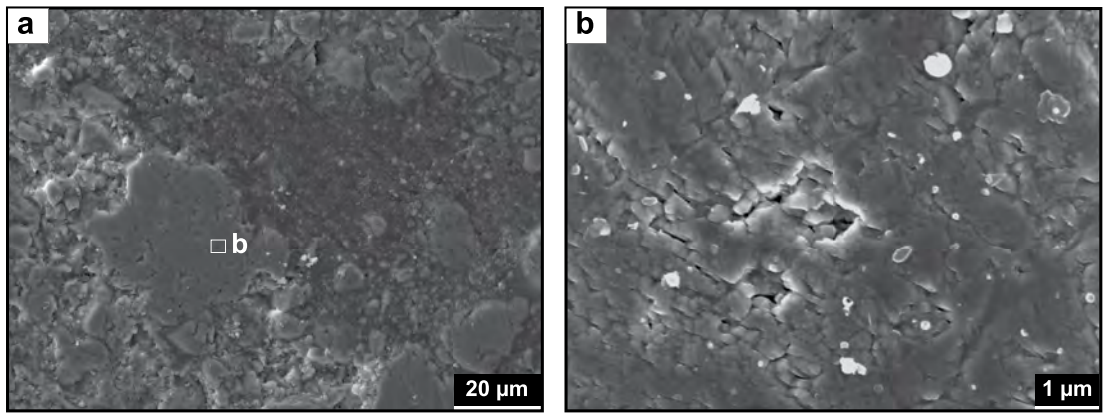

Figure 8. Top-view of fault mirror-like surface (MS, sample 5, 12 cm of slip). (a) MS made by smeared bitumen (dark gray) and dolostone clasts. (b) The MS is made of nanoparticles of dolomite glued by bitumen. SEM-SE images.

with lobate-cuspate grain boundaries immersed in a bitumen-rich matrix and topped by a 1 to 15–20 µm-thick layer of smeared bitumen (Figure 7f).

The MSs are thus defined by these thin layers of smeared bitumen and the exposed surfaces of (a) ultra-fine dolostone grains dispersed in the bitumen layers (Figures 7a, 7b, 7d, 7e, and 8), (b) dolostone grains composed by a thin layer of aggregate nanograins (Figure 8b), or (c) dolostone grains showing rough grain boundaries when in contact with bitumen (Figure 7d).

Some of the samples collected from faults that accommodated slip ≥12 cm present fragments of multiple slip zones. The thickness of the composite slip zone broadly increases with fault displacement. Evidence of fluid infiltration associated with calcite precipitation is also widespread (Figure 9). For instance, the fault core of a normal fault accommodating 12 cm of displacement (sample 5 in Figure 5) is composed of at least two slip zones (Figure 9a). The upper slip zone (probably the youngest) is ca. 100 µm thick, and it is made of angular to sub-rounded dolostone clasts (<50 µm in size) and few bitumen-rich clasts as well as clasts of previous dolostone cataclasites cemented by calcite (5–10 µm in size crystals; Figures 9a–9d). This upper slip zone is limited to the top by a MS and to the bottom by a lower slip zone locally developed on ∼20 µm bitumen layer (Figure 9a). The sharp boundary between the two slip zones is defined by flat grain boundaries of dolomite and calcite; the bitumen-rich layer contains ultra-fine grains of dolostone with elongated clasts aligned with the slip zone direction (Figures 9a and 9b), similar to the ones found in small displacement faults (Figure 7b). This layer is fragmented across the analyzed thin section and some fragments are embedded in the upper slip zone. Beneath the bitumen-rich layer of the lower slip zone, it is possible to observe an ultracataclasite made of dolostone grains immersed in a calcite-rich matrix (Figures 9a and 9b). The number of slip zones increases with displacement (sample 1 in Figure 5; 3.8 m of displacement), as attested in Figure 9e. Fragments of ultracataclasite made of indented grains of dolostone (from 10 to 1 µm in size) and bitumen, bounded by a sharp slip surface (Figures 9e and 9f) are embedded in a sparry calcite cement (Figure 9f).

6. Discussion

6.1. Compressional Versus Extensional Structures

The study area is characterized by the presence of structures related to a Late Miocene-Middle Pliocene compressional phase (i.e., syncline and asymmetric folds, verticalized bedding, reverse faults) cut and dissected by mainly NE-SW and E-W striking normal Middle Pliocene to Holocene faults.

The tilting and verticalization of the bituminous dolostone beds approaching the Monte Camicia Thrust (Figures 2 and 3) coupled with the presence of *Z*-type asymmetric parasitic folds along the east side of the studied gully (Stop 2 in Figures 2a and 4a–4c) can be interpreted as part of the limb of a decametric-in-scale synform fold, with the hinge buried beneath the valley and with a fold axis striking ca. E-W (Figure 2a). This interpretation is supported by the stratigraphic polarity of the bitumen-rich dolostone strata (Figure 3d). Therefore, the Monte Camicia Thrust would be responsible for the dragging, folding and verticalization of the strata of the bituminous dolostones during

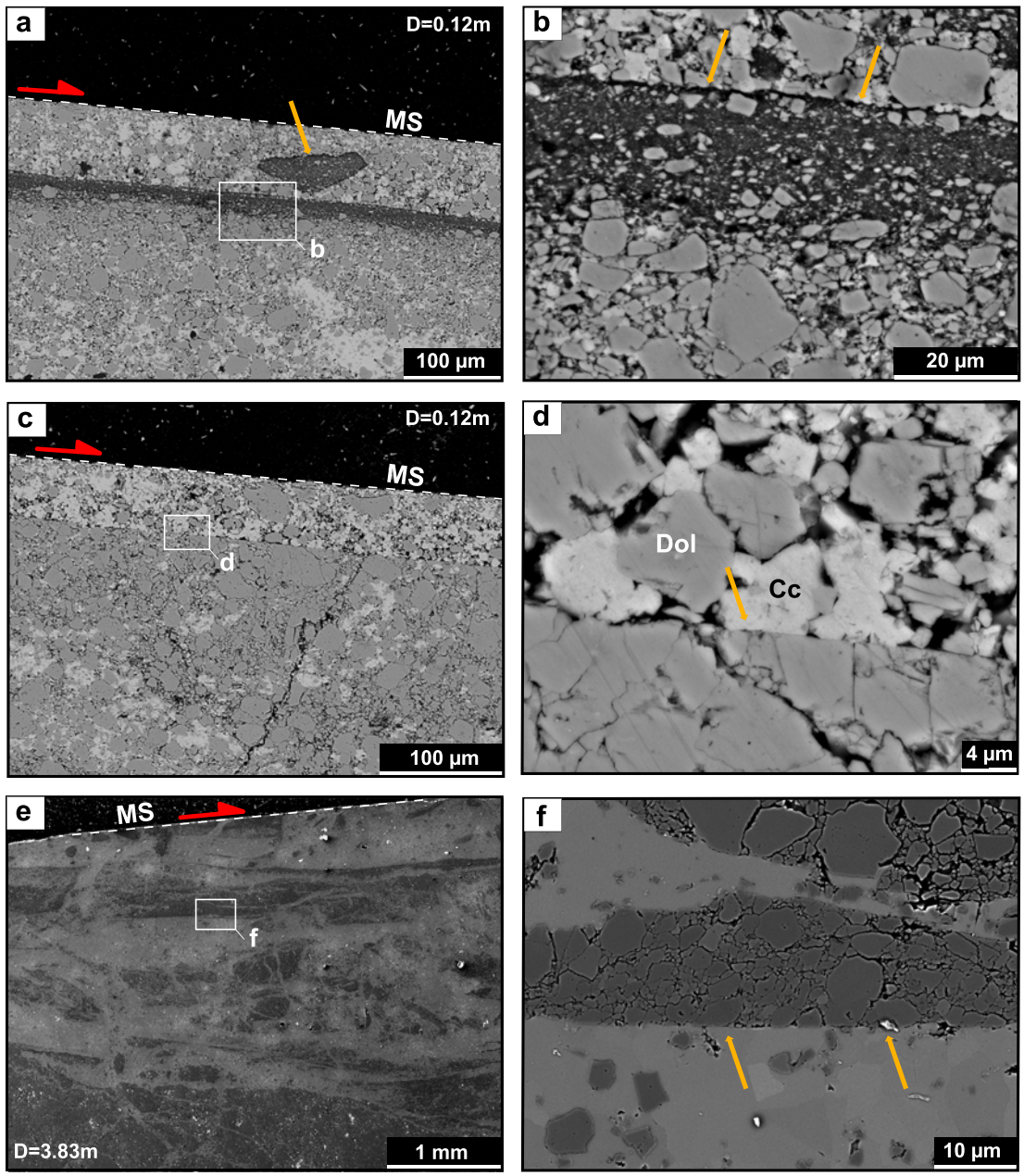

Figure 9. Slip zones and associated mirror surfaces from normal faults cutting bituminous dolostones. These slip zones recorded fluid infiltration (calcite precipitation). Panels (a–d) are from sample 5 (0.12 m of slip). (a) Two slip zones beneath the exposed mirror surface (mirror-like surface (MS)). The upper slip zone is dolomite (Dol; light gray) and calcite (Cc; white) rich and includes an angular fragment of an older bitumen-rich slip zone (dark gray; yellow arrow). The lower slip zone is bitumen-rich. The upper and lower slip zones are separated by an ultra-polished slip surface (see detail in b). (b) Bitumen-rich slip zone (yellow arrow) with dolostone clasts oriented with their long axis sub-parallel to the wall rocks. (c) The upper slip zone includes angular grains of dolostone and fragments of older slip zones cemented by calcite. (d) The contact of calcite with dolostone grains is very flat (see yellow arrow), suggesting the activation of pressure-solution processes. Panels (e) and (f) are from sample 1 (3.83 m of slip), which has multiple slip zones bounded by MSs. (e) The slip zones are fragmented and then cemented by calcite precipitation. (f) Detail of an older slip zone (yellow arrow) with sharp boundaries made of indented grains of dolostone. Grain indentation is due to pressure-solution processes. SEM-BSE images. *D* = displacement. Red arrow = shear sense.

the Miocene-Pliocene thrusting. Our interpretation supports the hypothesis that the Monte Camicia Thrust formed as an out-of-sequence thrust during the Pliocene (Ghisetti & Vezzani, 1986a, 1986b, 1991; Lucca et al., 2019) and placed the Jurassic-Cretaceous rudist calcarenites onto the Triassic bituminous dolostones. The younger-on-older geometry of this thrust can be explained by its propagation through an already folded stratigraphic sequence due to the activity of the lower and older Vado di Ferruccio Thrust (Ghisetti & Vezzani, 1991). The Vado di Ferruccio

Thrust itself has been interpreted as an original out-of-sequence during the complex spatio-temporal shortening history driven by the GSTS (Ghisetti & Vezzani, 1991; Lucca et al., 2019).

In the study area (Figure 2a), most of the normal faults strike NE-SW and E-W and accommodate only a few cm of displacement with dip-slip to transtensional kinematic (Figures 2a and 4c). These normal faults dip mainly at >55° toward the south and are associated with ultra-cataclastic slip zones bounded by mirror-like slip surfaces with smeared bitumen (Figures 4 and 5). Many normal faults cut the compressional structure described above and other crosscut each other (Figure 4). Based on the field evidence, we propose that while few and minor normal faults formed during the Monte Camicia Thrust activity, most formed during the subsequent extensional phase. These transtensional faults (Figure 2a) are probably related to the normal faulting, proposed by Ghisetti and Vezzani (1986a, 1986b), which cut with the same trend the hangingwall block of the Monte Camicia Thrust in the study area (Stop 1 and 3 in Figure 2a). Following Leah et al. (2018), in the geological cross-section (Figure 2a) we propose that normal faults dipping >60° toward S-SW and located in the northernmost part of the valley cut the Vado di Ferruccio Thrust, that bounds the thrust sheet of bituminous dolostones and truncates the *Corniola* limestones in its footwall (see Figures 2a and 2e in Leah et al., 2018). Furthermore, the dip angle of the southern and minor faults decreases toward the south so that these faults terminate gently on the thrust (Figure 2a). This interpretation implies the reactivation of the Vado di Ferruccio Thrust as a low-angle normal fault (see evidence in Leah et al., 2018).

6.2. Seismic Cycle Recorded in Bituminous Dolostones

The microstructural analysis conducted on the slip zones of normal faults reveals the activation of several deformation mechanisms. These mechanisms can be associated with the different phases of the seismic cycle (pre-seismic, co-seismic, post-seismic, and inter-seismic; Scholz, 2019), as illustrated in the conceptual model of Figure 10. In bitumen-rich slip zones a foliated fabric may be representative of the viscous behavior of bitumen that acts as a weak phase (Rutter et al., 2013) respect to the surrounding dolostone clasts. Elongated dolostone clasts within the bitumen-rich slip zones are oriented with the long axis parallel to the MSs (Figures 7b and 9b). This shape preferred orientation could be the result of fracturing of the dolostone grains in the wall rocks during the initial stages of slip, their progressive capture by the slip zone, and the orientation of the "rigid" particles during viscous flow (e.g., Cladouhos, 1999) in tandem with bitumen smearing and squeezing (inter-seismic or pre-seismic, Phase 1 in Figure 10). Viscous shear structures in bitumen-rich layers are observed in all the studied normal faults, independent of the accommodated displacement. Flow structures and porphyroclastic-like dolomitic aggregates in bitumen-rich layers are also found parallel to the bedding in the host rock away from normal faults. These viscous deformations potentially occurred at low strain rates throughout the burial and tectonic history (i.e., thrusting) of the bituminous dolostones (Figure 6). The occurrence of viscous flow localized in the proximity of MSs may indicate a "slow" (aseismic) deformation during inter-seismic and/or pre-seismic loading (Phase 1 in Figure 10).

Conversely, the slip zones of faults accommodating larger displacement include tabular fragments of previous slip zones with sharp edges probably corresponding to older MSs (based on roughness and similarities with the exposed ones) embedded in a new cataclastic layer or cemented by calcite precipitation (Figures 9a, 9c, 9e, and 9f). Following Lucca et al. (2019), this sparry calcite cement is precipitated from percolating carbonate-rich fluids meteoric in origin and infiltrated in the vadose zone during the extensional reactivation of the Monte Camicia Thrust. In these younger slip zones, the presence of fragments of bitumen-rich slip zones, which should record viscous flow deformation (Figures 9a and 9b; Cheung & Cebon, 1997; Trippetta & Geremia, 2019), suggests an abrupt co-seismic rupture and fast slip that could be the geological record of a co-seismic phase (Phase 2, Figure 10), followed by fluid infiltration. Fragments of bitumen can be found only in this slip zone, while in all the other fault samples and in the host rock, organic matter deforms by viscous flow. Fault strength recovery by calcite precipitation causes the hardening of the slip zone once the fault motion is halted during the post-seismic phase (Phase 3, Figure 10). Following this interpretation, whenever the slip zones of large faults are bounded by two MSs and include fragments of former bitumen-rich slip zones and/or fragments of other MSs and cataclastic calcite (as in Figure 9a and 9c), they would register multiple events of seismic rupture. Subsequently, ruptured faults sealed by calcite would undergo precipitation-hardening of the slip zone (e.g., Callahan et al., 2020; Di Toro & Pennacchioni, 2005; Tarasewicz et al., 2005; Woodcock et al., 2007). Hence, the slip associated with further seismic ruptures would be localized out of plane in the principal slip zone and reworks the existing cemented fault rocks (new co-seismic Phase 5 in Figure 10).

10.1029/2023GC011063

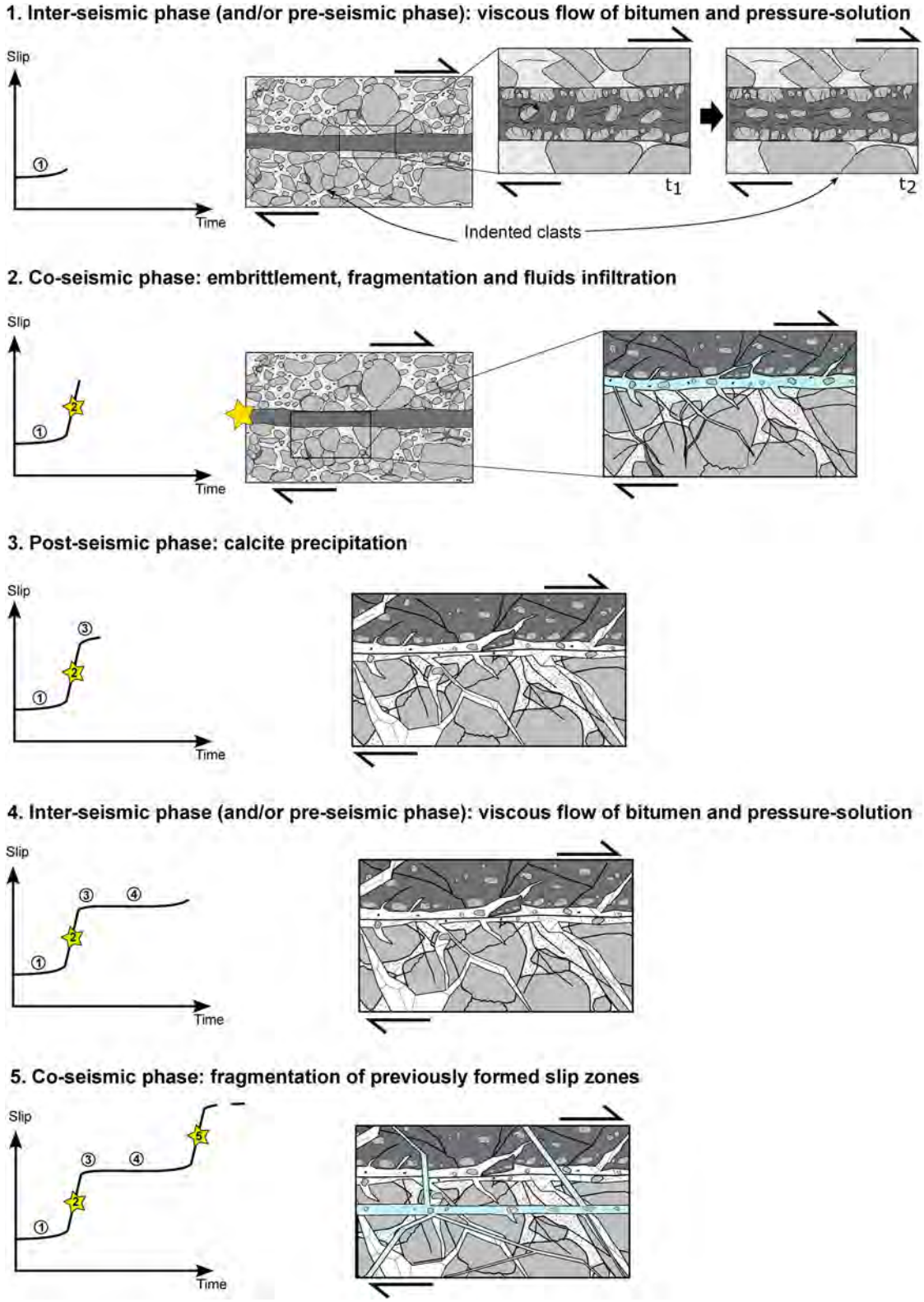

Figure 10.

As observed by Leah et al. (2018), the total length of normal and transtensive faults in the Fornaca Valley is difficult to assess but it is possible that some are tens to hundreds of meters-long with cm or even m of slip. Therefore, they could have hosted small earthquake ruptures ($M_w < 2$) compatible with multiple events recorded in our microstructures. Distributed seismicity along minor normal faults in a rock volume at shallow crustal depths is also consistent with the structure of normal seismic faults in the same region, as illuminated by small (down to $M_w = 0.7$) aftershocks after the l'Aquila M6.1 earthquake (Valoroso et al., 2014).

The percolation of calcite-enriched, meteoric fluids through seismically active faults has been extensively documented in the Northern and Central Apennines (Agosta & Kirschner, 2003; Smeraglia et al., 2021) and is also consistent with our observations of cemented slip zones of normal faults (Figure 9).

Dolostone clasts in the ultracataclasites of large faults have lobate-cuspate grain boundaries typical of stylolites, further evidence of the activation of viscous pressure-solution processes after cataclastic fragmentation (Figures 7d–7f and 9f). The occurrence of bitumen-rich stylolites in the wall rocks with the orientation of the foliation (i.e., perpendicular to the maximum shortening direction) consistent with the normal sense of shear (top to the right in Figure 7c) is also in agreement with the activation of pressure-solution processes (Figure 7c). Transgranular fracturing during the co-seismic phase and the subsequent increase in the permeability of the slip zone can accelerate the kinetics of pressure-solution in the post-seismic phase by opening pathways for diffusion mass transfer until these fractures are closed during fault recovery (Gratier et al., 1999; Renard et al., 2000; Phase 4 in Figure 10). Furthermore, the presence of organic matter in the cataclastic matrix (Figure 7d) (i.e., an insoluble phase) increases the dissolution rate along the mutual contacts between dolomite and calcite and bitumen with contrasting solubility and by the preservation of water films (Gratier & Gueydan, 2007; Gratier et al., 2013). This body of evidence suggests that the pressure-solution process is widespread in these faults and acted at different dissolution rates both before and after the fragmentation of old slip zones and the formation of new ones by co-seismic fracturing in a fluid-rich environment.

6.3. Formation of Mirror-Like Surfaces

A prominent structural feature in the area is the abundance of exposed MSs, independent of the displacement accommodated by the associated fault/fracture (Figures 4d–4g and 5). In all the studied slip zones, the MSs sharply "truncate" the dolomitic grains (samples 7, 8, 9 in Figure 5; Figures 7a, 7e, and 9c–9e). MSs are most prominent and continuous in large displacement faults; however, some MSs are found in faults/fractures often with wavy or bent surfaces (perpendicular and parallel to slip direction) that accommodate less than 1 mm of displacement, or along the bedding interface of folded strata (i.e., flexural slip surfaces Figure 4b; sample 6 in Figure 5). Continuous, sharp mirror-like fault surfaces truncating clasts were obtained in dry experiments performed on pure dolostones gouges sheared at seismic slip rates under low normal stresses (up to 27 MPa) by Fondriest et al. (2013). In addition, the shattered rudist calcarenites located in the hangingwall of the Monte Camicia Thrust are similar to in situ shattered carbonates found in damage zones of other faults with clear evidence of seismogenic history (Demurtas et al., 2016; Fondriest et al., 2015, 2020). This evidence suggests that the studied faults accommodated seismic slip at some stage during their activity (see Section 6.2).

Moreover, several microstructures outline the MSs can be interpreted as the result of pressure-solution processes (e.g., indentation and flattening of dolostone grains, Figure 9d) or viscous flow (smeared bitumen, Figure 8a), which is typical of "aseismic" creep deformation (Gratier et al., 2011, 2013). As a matter of fact, MSs outlined by nanoparticles have also been produced in experiments performed at sub-seismic slip rates (≈0.1–10 μm/s; see Section 1). Proposed mechanisms for the formation of seismic and aseismic MSs are (a) localized dynamic recrystallization due to frictional heating during seismic deformation conditions (Smith et al., 2013), (b) formation of

Figure 10. Conceptual model of the seismic cycle in faults cutting bituminous dolostones based on field and microstructural observations discussed in this study. (**1**) **Inter-seismic phase (and/or pre-seismic phase)**: dissolution of dolostone grains and viscous flow of bitumen in the slip zone. Viscous flow causes clast rotation (see the vorticity arrow in *t*1) and the development of a shape preferred orientation of the dolostone clasts (e.g., Figure 7b). These processes also contribute to the formation of mirror-like fault surfaces (Verberne et al., 2019). (**2**) **Co-seismic phase**: co-seismic rupture in a fluid-rich environment causes fragmentation of both dolostone and bitumen and fluid percolation/infiltration (e.g., Figure 9a). Co-seismic slip may also contribute to the formation of mirror-like fault surfaces (Fondriest et al., 2013). (**3**) **Post-seismic phase**: calcite precipitation from percolating fluids and pressure-solution deformation causes fault strength recovery and hardening of the slip zones and of the damaged fault rocks (e.g., Figure 9d). (**4**) **Inter-seismic phase (and/or pre-seismic phase)**: dissolution of dolostone grains and viscous flow of bitumen in the slip zone. (**5**) **Co-seismic phase**: seismic ruptures propagate along sealed and hardened faults. Previously formed slip zones are cut by the newly formed slip zones (e.g., Figure 9e).

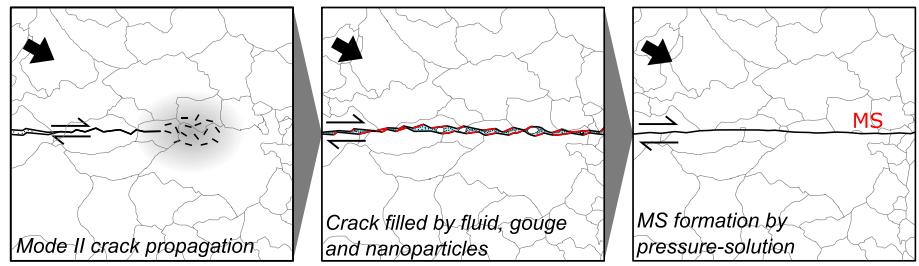

Figure 11. New model of mirror-like surface formation proposed in this work. Propagation of mode II transgranular crack results in gouge and nanoparticle formation that in the presence of a fluid phase (water) can smooth the edges of the crack by pressure-solution. The thick arrow shows the orientation of the maximum principal stress, σ_1.

nanograins by strain-induced plasticity followed by brittle fracturing of crystals and abrasion at very small scales during aseismic, sub-seismic and seismic deformation (Siman-Tov et al., 2013; Tesei et al., 2017; Verberne et al., 2014). Pozzi et al. (2018) suggest that MSs are not frictional slip surfaces, but mark the broken boundaries between strong, sintered wall rocks and a weak and viscously deforming principal slip zone.

Based on the field and microstructural evidence listed above, we propose an alternative mechanism for MSs formation at these shallow crustal depths (1–4 km) and low temperature (<100°C, see Section 2.2) conditions in the presence of fluids. These conditions are quite common in carbonate-built mountain belts, especially in the Apennines, where polished slip surfaces are widespread (Demurtas et al., 2016; Fondriest et al., 2012, 2015; Jackson & McKenzie, 1999; Leah et al., 2018; Ohl et al., 2020; Siman-Tov et al., 2013). The proposed mechanism includes (a) propagation of mode II transgranular cracks through the intact bare rock forming two rough fracture surfaces filled by gouge and nanoparticles that are in contact through highly stressed asperities (Figure 11, stage 1) and, (b) ingression of a fluid phase (carbonated water) that triggers the reduction of fracture roughness (at the micro and nanoscale) by the dissolution or by cold sintering of nanoparticles and asperities (Figure 11, stage 2). This "static" flattening of rough surfaces and slip zones may operate along faults and fractures during the inter-seismic period (Figure 11, stage 3). The proposed mechanism would help explain the observation of Ms along faults with negligible slip displacements.

The high bitumen-content, the low temperature of the fluid (<80°C), and abundance of micro-cracks (e.g., Figure 7a) would increase the rate and effectiveness of the dissolution of dolomite (Gratier & Gueydan, 2007). The above mechanism possibly operates during the inter-seismic/post-seismic phases at shallow crustal depths and could reduce the surface roughness also in the case of slip zones of large displacement faults that potentially experienced seismic rupture (e.g., Figure 9).

This series of processes could result in the formation, during fault quasi-stationary phases, of extensive patches of ultra-polished and even *striae*-free MSs (Figure 5). According to this model, the MSs can represent the ultra-flattened or dissolved surface of a major rock discontinuity, such as a fracture, a fault, or flexural slip surface and may not always be associated with seismic slip displacement. Nevertheless, the studied mirrors are developed on a very peculiar rock type; smearing of bitumen (which occur not only in the slip zone, but also in the host rock, probably during burial) can smooth out the irregularities and fill in the grooves, contributing to the formation of smooth rock surfaces at aseismic slip rates without significant amount of displacement.

7. Conclusions

In this study, we present new field data regarding the structure and kinematics of the Monte Camicia Thrust (Figures 2–4), and microstructural investigations of slip zones and fault/fracture MSs cutting bituminous dolostones at its footwall (Figures 5–9). Based on the interpretation of the microstructures, the rheology of these faults is controlled by the interplay of cataclasis, fluid flow and viscous flow of bitumen spread over the slip surfaces and within the slip zones. Faults may register aseismic deformation occurring via cataclastic flow aided by the viscous rheology of bitumen and by pressure-solution, which may also aid the formation of MSs (inter-seismic/pre-seismic or inter-seismic/post-seismic phase). However, in larger faults, the presence of fragments of older slip zones, of bitumen-rich clasts and of slip zones cemented by calcite suggests the occurrence of multiple seismic ruptures in the presence of carbonate-rich fluids (co-seismic phase, 1 and 3 in Figure 10).

Mirror-like surfaces, extremely common in the area, are found in both large faults and in faults/fractures with negligible displacement: we suggest that they may form by a combination of (a) dissolution of fine dolostone grains formed during crack propagation or fault slip (Figure 11) and (b) bitumen smearing causing flattening of fracture roughness.

As a consequence, the microstructures found in the slip zones and surface mirrors cutting the bituminous dolostones in the Fornaca Valley capture the main phases of the seismic cycle, including rapid co-seismic slip, viscous flow and fault strength recovery during post-seismic and inter-seismic phases (1, 3, and 4 in Figure 10).

Data Availability Statement

The structural data supporting this work are publicly available online (Chinello et al., 2023).

Acknowledgments
This research was founded by a INGV PhD grant: "*Formation of polished surfaces in natural rocks: experimental and field constraints*" (MC), and by the European Research Council Consolidator Grant Project NOFEAR No 614705 (MF, RG, and GDT). MF received funding from NextGenerationEU (REACT project) and from the 2021 STARS Grants@Unipd programme (STIFF project). The authors thank Renato Raineri for fieldwork activities, Leonardo Tauro and Silvia Cattò for thin sections preparation, Stefano Castelli for the high-resolution hand sample photographs, Manuela Nazzari, Giorgio Pennacchioni and Jacopo Nava for SEM support, Elena Spagnuolo and Sveva Corrado for the constructive discussions. The authors thank the editor Claudio Faaccenna, Jean-Pierre Gratier and an anonymous reviewer for their extremely constructive feedback. Open access funding provided by Università degli Studi di Padova within the CARE-CRUI agreement.

References

Adamoli, L., Bigozzi, A., Ciarapica, G., Cirilli, S., Passeri, L., Romano, A., et al. (1990). Upper Triassic Bituminous facies and Hettangian pelagic facies in the Gran Sasso range. *Bollettino della Societa Geologica Italiana*, *109*, 219–230.

Adamoli, L., Calamita, F., & Pizzi, A. (2012). *Note illustrative Della Carta Geologica D'Italia Alla Scala 1:50,000, Foglio 349* "Gran Sasso d'Italia". Ispra.

Adamoli, L., Mancinelli, A., Pieruccini, U., & Romano, A. (1984). Ricerche Geologiche Sul Gran Sasso d'Italia (Abruzzo). VIII. Età e Significato Paleoambientale Degli 'Scisti Bituminosi'. *Studi Geologici Camerti*, *IX*, 7–14.

Agosta, F., & Aydin, A. (2006). Architecture and deformation mechanism of a basin-bounding normal fault in Mesozoic platform carbonates, central Italy. *Journal of Structural Geology*, *28*(8), 1445–1467. https://doi.org/10.1016/j.jsg.2006.04.006

Agosta, F., & Kirschner, D. L. (2003). Fluid conduits in carbonate-hosted seismogenic normal faults of Central Italy. *Journal of Geophysical Research*, *108*(B4), 2221. https://doi.org/10.1029/2002jb002013

Allmendinger, R. W., Cardozo, N., & Fisher, D. (2012). *Structural geology algorithms: Vectors and tensors in structural geology* (p. 289). Cambridge University Press.

Aretusini, S., Núñez-Cascajero, A., Spagnuolo, E., Tapetado, A., Vázquez, C., & Di Toro, G. (2021). Fast and localized temperature measurements during simulated earthquakes in carbonate rocks. *Geophysical Research Letters*, *48*(9), e2020GL091856. https://doi.org/10.1029/2020GL091856

Atkinson, B. K., & Meredith, P. G. (1987). The theory of subcritical crack growth with applications to minerals and rocks. *Fracture Mechanics of Rock*, *2*, 111–166. https://doi.org/10.1016/b978-0-12-066266-1.50009-0

Baccheschi, P., De Gori, P., Villani, F., Trippetta, F., & Chiarabba, C. (2019). The preparatory phase of the M_w 6.1 2009 L'Aquila (Italy) normal faulting earthquake Traced by foreshock Time-Lapse Tomography. *Geology*, *48*(1), 49–55. https://doi.org/10.1130/g46618.1

Balsamo, F., Aldega, L., De Paola, N., Faoro, I., & Storti, F. (2014). The signature and mechanics of earthquake ruptures along shallow creeping faults in poorly lithified sediments. *Geology*, *42*(5), 435–438. https://doi.org/10.1130/g35272.1

Barchi, M., & Bigozzi, A. (1995). Ipotesi Sulla Geometria e La Genesi Dei Bacini Euxinici Del Trias Superiore in Appennino Centrale. *Studi Geologici Camerti, Speciale*, *1*, 53–62.

Bertinelli, A., Nannarone, C., Passeri, L., & Venturi, F. (2004). Hettangian ammonites and radiolarians in the Mt. Camicia (Gran Sasso, Central Apennines). *Rivista Italiana di Paleontologia e Stratigrafia*, *110*(1), 87–95.

Billi, A., & Di Toro, G. (2008). Fault-Related carbonate rocks and earthquake indicators: Recent advances and future trends. In S. J. Landowe & G. M. Hammler (Eds.), *Structural geology: New research*. Novascience.

Billi, A., Salvini, F., & Storti, F. (2003). The damage zone-fault core transition in carbonate rocks: Implications for fault growth, structure and permeability. *Journal of Structural Geology*, *25*(11), 1779–1794. https://doi.org/10.1016/s0191-8141(03)00037-3

Boneh, Y., Sagy, A., & Reches, Z. (2013). Frictional strength and wear-rate of carbonate faults during high-velocity, steady-state sliding. *Earth and Planetary Science Letters*, *381*, 127–137.

Caine, J. S., Evans, J. P., & Forster, C. B. (1996). Fault zone architecture and permeability structure. *Geology*, *24*(11), 1025–1028. https://doi.org/10.1130/0091-7613(1996)024<1025:fzaaps>2.3.co;2

Calamita, F., Ben M'Barek, M., Di Vincenzo, M., & Pelorosso, M. (2004). *The Pliocene thrust system of the Gran Sasso salient (Central Apennines, Italy)* (pp. 227–234). Mapping Geology in Italy, SELCA.

Calamita, F., Scisciani, V., Adamoli, L., BenM'Barek, M., & Pelorosso, M. (2002). Il Sistema a thrust del Gran Sasso d'Italia (Appennino Centrale). *Studi Geologici Camerti*, *1*, 19–32.

Callahan, O. A., Eichhubl, P., & Davatzes, N. C. (2020). Mineral precipitation as a mechanism of fault core growth. *Journal of Structural Geology*, *140*, 104156. https://doi.org/10.1016/j.jsg.2020.104156

Cardello, G. L., & Doglioni, C. (2015). From mesozoic rifting to Apennine Orogeny: The Gran Sasso range (Italy). *Gondwana Research*, *27*(4), 1307–1334. https://doi.org/10.1016/j.gr.2014.09.009

Cardozo, N., & Allmendinger, R. W. (2013). Spherical projections with OSXStereonet. *Computers & Geosciences*, *51*, 193–205. https://doi.org/10.1016/j.cageo.2012.07.021

Centamore, E., Fumanti, F., & Nisio, S. (2002). The Central-Northern Apennines Geological evolution from Triassic to Neogene Time. *Bollettino della Societa Geologica Italiana*, *1*(1), 181–197.

Chen, X., Madden, A. S., Bickmore, B. R., & Reches, Z. (2013). Dynamic weakening by nanoscale smoothing during high-velocity fault slip. *Geology*, *41*(7), 739–742. https://doi.org/10.1130/g34169.1

Cheung, C. Y., & Cebon, D. (1997). Experimental study of pure bitumens in tension, compression, and shear. *Journal of Rheology*, *41*(1), 45–74. https://doi.org/10.1122/1.550858

Chiarabba, C., Amato, A., Anselmi, M., Baccheschi, P., Bianchi, I., Cattaneo, M., et al. (2009). The 2009 L'Aquila (central Italy) M_w 6.3 earthquake: Main shock and aftershocks. *Geophysical Research Letters*, *36*(18), L18308. https://doi.org/10.1029/2009gl039627

Chiaraluce, L. (2012). Unravelling the complexity of Apenninic extensional fault systems: A review of the 2009 L'Aquila earthquake (Central Apennines, Italy). *Journal of Structural Geology*, *42*, 2–18. https://doi.org/10.1016/j.jsg.2012.06.007

Chiaraluce, L., Di Stefano, R., Tinti, E., Scognamiglio, L., Michele, M., Casarotti, E., et al. (2017). The 2016 Central Italy seismic sequence: A first look at the mainshocks, aftershocks, and source models. *Seismological Research Letters*, *88*(3), 757–771. https://doi.org/10.1785/0220160221

Chiaraluce, L., Valoroso, L., Piccinini, D., Di Stefano, R., & De Gori, P. (2011). The anatomy of the 2009 L'Aquila normal fault system (central Italy) imaged by high resolution foreshock and aftershock locations. *Journal of Geophysical Research Letters*, *116*(B12), B12311. https://doi.org/10.1029/2011JB008352

Chinello, M., Bersan, E., Fondriest, M., Tesei, T., Gomila, R., & Di Toro, G. (2023). Seismic cycle in bituminous dolostones (Monte Camicia thrust, Central Apennines, Italy) [Dataset]. Research Data Unipd. https://doi.org/10.25430/researchdata.cab.unipd.it.00000893

Cirella, A., Piatanesi, A., Cocco, M., Tinti, E., Scognamiglio, L., Michelini, A., et al. (2009). Rupture history of the 2009 L'Aquila (Italy) earthquake from non-linear joint inversion of strong motion and GPS data. *Geophysical Research Letters*, *36*(19), L19304. https://doi.org/10.1029/2009GL039795

Cladouhos, T. T. (1999). Shape preferred orientations of survivor grains in fault gouge. *Journal of Structural Geology*, *21*(4), 419–436. https://doi.org/10.1016/S0191-8141(98)00123-0

Cocco, M., Chiarabba, C., Di Bona, M., Selvaggi, G., Margheriti, L., Frepoli, A., et al. (1999). The April 1996 Irpinia seismic sequence: Evidence for fault interaction. *Journal of Seismology*, *3*(1), 105–117. https://doi.org/10.1023/a:1009771817737

Collettini, C., Barchi, M. R., De Paola, N., Trippetta, F., & Tinti, E. (2022). Rock and fault rheology explain differences between on fault and distributed seismicity. *Nature Commuications*, *13*(1), 5627. https://doi.org/10.1038/s41467-022-33373-y

Collettini, C., Carpenter, B. M., Viti, C., Cruciani, F., Mollo, S., Tesei, T., et al. (2014). Fault structure and slip localization in carbonate-bearing normal faults: An example from the Northern Apennines of Italy. *Journal of Structural Geology*, *67*, 154–166. https://doi.org/10.1016/j.jsg.2014.07.017

Collettini, C., Viti, C., Tesei, T., & Mollo, S. (2013). Thermal decomposition along natural carbonate faults during earthquakes. *Geology*, *41*(8), 927–930. https://doi.org/10.1130/g34421.1

Cowan, D. S. (1999). Do faults preserve a record of seismic slip? A field geologist's opinion. *Journal of Structural Geology*, *8*(21), 995–1001. https://doi.org/10.1016/s0191-8141(99)00046-2

Cox, S. F. (1995). Faulting processes at high fluid pressures: An example of fault valve behaviour form the Waddle Gully fault, Victoria, Australia. *Journal of Geophysical Research*, *100*(B7), 12841–12859. https://doi.org/10.1029/95jb00915

D'Agostino, N., Chamot-Rooke, N., Funiciello, R., Jolivet, L., & Speranza, F. (1998). The role of pre-existing thrust faults and Topography on the styles of extension in the Gran Sasso range (Central Italy). *Tectonophysics*, *292*(3–4), 229–254. https://doi.org/10.1016/S0040-1951(98)00070-5

Delle Piane, C., Clennell, M. B., Keller, J. V. A., Giwelli, A., & Luzin, V. (2017). Carbonate hosted fault rocks: A review of structural and microstructural characteristic with implications for seismicity in the upper crust. *Journal of Structural Geology*, *103*, 17–36. https://doi.org/10.1016/j.jsg.2017.09.003

Demurtas, M., Fondriest, M., Balsamo, F., Clemenzi, L., Storti, F., Bistacchi, A., & Di Toro, G. (2016). Structure of a normal seismogenic fault zone in Carbonates: The Vado Di Corno fault, Campo Imperatore, Central Apennines (Italy). *Journal of Structural Geology*, *90*, 185–206. https://doi.org/10.1016/j.jsg.2016.08.004

De Paola, N., Holdsworth, R. E., Viti, C., Collettini, C., & Bullock, R. (2015). Can grain size sensitive flow lubricate faults during the initial stages of earthquake propagation? *Earth and Planetary Science Letters*, *431*, 48–58. https://doi.org/10.1016/j.epsl.2015.09.002

Di Toro, G., Mittempergher, S., Ferri, F., Mitchell, T. M., & Pennacchioni, G. (2012). The contribution of structural geology, experimental rock deformation and numerical modelling to an improved understanding of the seismic cycle: Preface to the Special Volume "Physico-chemical processes in seismic faults",. *Journal of Structural Geology*, *38*, 3–10. https://doi.org/10.1016/j.jsg.2012.01.025

Di Toro, G., & Pennacchioni, G. (2005). Fault plane processes and mesoscopic structure of a strong-type seismogenic fault in tonalites (Adamello batholith, Southern Alps). *Tectonophysics*, *402*(1–4), 55–80. https://doi.org/10.1016/j.tecto.2004.12.036

Faulkner, D. R., Jackson, C. A. L., Lunn, R. J., Schlische, R. W., Wibberley, C. A. J., & Withjack, M. O. (2010). A review of recent developments concerning the structure, mechanics and fluid flow properties of fault zones. *Journal of Structural Geology*, *32*(11), 1557–1575. https://doi.org/10.1016/j.jsg.2010.06.009

Finetti, I., Russi, M., & Slejko, D. (1979). The Friuli earthquake (1976–1977). *Tectonophysics*, *53*(3–4), 261–272. https://doi.org/10.1016/0040-1951(79)90070-2

Fondriest, M., Aretusini, S., Di Toro, G., & Smith, S. A. F. (2015). Fracturing and rock pulverization along an exhumed seismogenic fault zone in dolostones: The Foiana fault zone (southern Alps, Italy). *Tectonophysics*, *654*, 56–74. https://doi.org/10.1016/j.tecto.2015.04.015

Fondriest, M., Balsamo, F., Bistacchi, A., Clemenzi, L., Demurtas, M., Storti, F., & Di Toro, G. (2020). Structural complexity and mechanics of a shallow crustal seismogenic source (Vado di Corno Fault Zone, Italy). *Journal of Geophysical Research: Solid Earth*, *125*(9), e2019JB018926. https://doi.org/10.1029/2019JB018926

Fondriest, M., Smith, S. A. F., Candela, T., Nielsen, S. B., Mair, K., & Di Toro, G. (2013). Mirror-like faults and power dissipation during earthquakes. *Geology*, *41*(11), 1175–1178. https://doi.org/10.1130/G34641.1

Fondriest, M., Smith, S. A. F., Di Toro, G., Zampieri, D., & Mittempergher, S. (2012). Fault zone structure and seismic slip localization in dolostones, an example from the Southern Alps, Italy. *Journal of Structural Geology*, *45*, 52–67. https://doi.org/10.1016/j.jsg.2012.06.014

Galadini, F., & Galli, P. (2000). Active tectonics in the Central Appennines (Italy)—Input data for seismic hazard assessment. *Natural Hazards*, *22*(3), 225–268. https://doi.org/10.1023/A:1008149531980

Ghisetti, F. (1987). Mechanisms of thrust faulting in the Gran Sasso Chain, Central Apennines, Italy. *Journal of Structural Geology*, *9*(8), 955–967. https://doi.org/10.1016/0191-8141(87)90004-6

Ghisetti, F., & Vezzani, L. (1986a). Assetto Geometrico Ed Evoluzione Strutturale Della Catena Del Gran Sasso Tra Vado Di Siella e Vado Di Corno. *Bollettino della Società Geologica Italiana e del Servizio Geologico d'Italia*, *105*, 131–171.

Ghisetti, F., & Vezzani, L. (1986b). Carta Geologica del Gruppo M.Siella-M.Camicia-M.Prena-M.Brancastello (Gran Sasso d'Italia, Abruzzo). Scale 1:15.000.

Ghisetti, F., & Vezzani, L. (1991). Thrust belt development in the Central Apennines (Italy): Northward polarity of thrusting and out-of-Sequence deformations in the Gran Sasso Chain. *Tectonics*, *10*(5), 904–919. https://doi.org/10.1038/s41407-022-0858-2

Ghisetti, F., & Vezzani, L. (1997). Geometrie deformative Ed Evoluzione Cinematica Dell'Appennino Centrale. *Studi Geologici Camerti, XIV*, 127–154.

Govorčin, M., Wdowinski, S., Matoš, B., & Funning, G. J. (2020). Geodetic source modelling of the 2019 M_w 6.3 Durrës, Albania, earthquake: Partial rupture of a blind reverse fault. *Geophysical Research Letters*, *47*, e2020GL088990. https://doi.org/10.1029/2020GL088990

Gratier, J.-P., Dysthe, D. K., & Renard, F. (2013). The role of pressure solution Creep in the ductility of the Earth's Upper Crust. *Advances in Geophysics*, *54*, 47–179. https://doi.org/10.1016/B978-0-12-380940-7.00002-0

Gratier, J.-P., Favreau, P., Renard, F., & Pili, E. (2002). Fluid pressure evolution during the earthquake cycle controlled by fluid flow and pressure solution crack sealing. *Earth Planets and Space*, *54*(11), 1139–1146. https://doi.org/10.1186/bf03353315

Gratier, J.-P., & Gueydan, F. (2007). Deformation in the presence of fluids and mineral reactions. Effect of fracturing and fluid-rock interaction on seismic Cycles. In *Tectonic faults: Agents of Change on a dynamic Earth* (pp. 319–356). MIT Press. https://doi.org/10.7551/mitpress/6703.003.0014

Gratier, J.-P., Menegon, L., & Renard, F. (2023). Pressure solution grain boundary sliding as a large strain mechanism of superplastic flow in the upper crust. *Journal of Geophysical Research: Solid Earth*, *128*(4), e2022JB026019. https://doi.org/10.1029/2022JB026019

Gratier, J.-P., Renard, F., & Labaume, P. (1999). How pressure solution creep and fracturing processes interact in the upper crust to make it behave in both a brittle and viscous manner. *Journal of Structural Geology*, *21*(8–9), 1189–1197. https://doi.org/10.1016/s0191-8141(99)00035-8

Gratier, J.-P., Richard, J., Renard, F., Mittempergher, S., Doan, M.-L., Di Toro, G., et al. (2011). Aseismic sliding of active faults by pressure solution Creep: Evidence from the san Andreas fault observatory at depth. *Geology*, *39*(12), 1131–1134. https://doi.org/10.1130/G32073.1

Hadizadeh, J. (1994). Interaction of cataclasis and pressure solution in a low-temperature carbonate shear zone. *Pure and Applied Geophysics*, *143*(1–3), 255–280. https://doi.org/10.1007/bf00874331

Improta, L., Latorre, D., Margheriti, L., Nardi, A., Marchetti, A., Lombardi, A. M., et al. (2019). Multi-segment rupture of the 2016 Amatrice-Visso-Norcia seismic sequence (central Italy) constrained by the first high-quality catalog of Early Aftershocks. *Scientific Reports*, *9*(1), 6921. https://doi.org/10.1038/s41598-019-43393

Jackson, J., & McKenzie, D. (1999). A hectare of fresh striations on the Arkitsa Fault, central Greece. *Journal of Structural Geology*, *21*, 1–6. https://doi.org/10.1016/S0191-8141(98)00091-1

Katz, B. J., Dittmar, E. I., & Ehret, G. E. (2000). A geochemical review of carbonate source rocks in Italy. *Journal of Petroleum Geology*, *23*(4), 399–424. https://doi.org/10.1111/j.1747-5457.2000.tb00494.x

Kennedy, L. A., & White, J. C. (2001). Low-temperature recrystallization in calcite: Mechanisms and consequences. *Geology*, *29*(11), 1027–1030. https://doi.org/10.1130/0091-7613(2001)029<1027:LTRICM>2.0.CO;2

Kim, Y.-S., Peacock, D. C. P., & Sanderson, D. J. (2004). Fault damage zones. *Journal of Structural Geology*, *26*(3), 503–517. https://doi.org/10.1016/j.jsg.2003.08.002

Koopman, A. (1983). Detachment tectonics in the Central Apennines, Italy. *Geologica Ultraiectina*, *30*, 1–155.

Leah, H., Fondriest, M., Lucca, A., Storti, F., Balsamo, F., & Di Toro, G. (2018). Coseismic extension recorded within the damage zone of the Vado di Ferruccio thrust fault, Central Apennines, Italy. *Journal of Structural Geology*, *114*, 121–138. https://doi.org/10.1016/j.jsg.2018.06.015

Lucca, A., Storti, F., Balsamo, F., Clemenzi, L., Fondriest, M., Burgess, R., & Di Toro, G. (2019). From submarine to subaerial out-of-sequence thrusting and Gravity-driven extensional faulting: Gran Sasso massif, Central Apennines, Italy. *Tectonics*, *38*(12), 4155–4184. https://doi.org/10.1029/2019TC005783

Masoch, S., Fondriest, M., Preto, N., Secco, M., & Di Toro, G. (2019). Seismic cycle recorded in cockade-bearing faults (Col de Teghime, Alpine Corsica). *Journal of Structural Geology*, *129*, 103889. https://doi.org/10.1016/j.jsg.2019.103889

Mastalerz, M., Drobniak, A., & Stankiewicz, A. B. (2018). Origin, properties, and implications of solid bitumen in source-rock reservoirs: A review. *International Journal of Coal Geology*, *195*, 14–36. https://doi.org/10.1016/j.coal.2018.05.013

Ohl, M., Plümper, O., Chatzaras, V., Wallis, D., Vollmer, V., & Drury, M. (2020). Mechanisms of fault mirror formation and fault healing in Carbonate rocks. *Earth and Planetary Science Letters*, *530*, 115886. https://doi.org/10.1016/j.epsl.2019.115886

Pace, P., Domenica, A. D., & Calamita, F. (2014). Summit low-angle faults in the Central Apennines of Italy: Younger-on-older thrusts or rotated normal faults? Constraints for defining the tectonic style of thrust belts. *Tectonics*, *33*(5), 756–785. https://doi.org/10.1002/2013tc003385

Papadopoulos, G. A., Agalos, A., Carydis, P., Lekkas, E., Mavroulis, S., & Triantafyllou, I. (2020). The 26 November 2019 M_w 6.4 Albania destructive earthquake,. *Seismological Research Letters*, *91*(6), 3129–3138. https://doi.org/10.1785/0220200207

Parry, W. T., & Bruhn, R. L. (1990). Fluid pressure transients on seismogenic normal faults. *Tectonophysics*, *179*(3–4), 335–344. https://doi.org/10.1016/0040-1951(90)90299-n

Passelègue, F. X., Aubry, J., Nicolas, A., Fondriest, M., Deldicque, D., Schubnel, A., & Di Toro, G. (2019). From fault creep to slow and fast earthquakes in carbonates. *Geology*, *47*(8), 744–748. https://doi.org/10.1130/G45868.1

Pizzi, A., Di Domenica, A., Gallovič, F., Luzi, L., & Puglia, R. (2017). Fault segmentation as constraint to the occurrence of the main shocks of the 2016 Central Italy seismic sequence. *Tectonics*, *36*(11), 2370–2387. https://doi.org/10.1002/2017TC004652

Pozzi, G., De Paola, N., Holdsworth, R. E., Bowen, L., Nielsen, S. B., & Dempsey, E. D. (2019). Coseismic ultramylonites: An investigation of nanoscale viscous flow and fault weakening during seismic slip. *Earth and Planetary Science Letters*, *516*, 164–175. https://doi.org/10.1016/j.epsl.2019.03.042

Pozzi, G., De Paola, N., Nielsen, S. B., Holdsworth, R. E., & Bowen, L. (2018). A new interpretation for the nature and significance of mirror-like surfaces in experimental Carbonate-hosted seismic faults. *Geology*, *46*(7), 583–586. https://doi.org/10.1130/G40197.1

Ramsay, J. G., & Huber, M. I. (1987). Folds and fractures. In *The techniques of Modern structural geology* (Vol. 2, pp. 309–700). Academic Press.

Renard, F., Gratier, J.-P., & Jamtveit, B. (2000). Kinetics of crack-sealing, intergranular pressure solution, and compaction around active faults. *Journal of Structural Geology*, *22*(10), 1395–1407. https://doi.org/10.1016/s0191-8141(00)00064-x

Rowe, C. D., & Griffith, W. A. (2015). Do faults preserve a record of seismic slip: A second opinion. *Journal of Structural Geology*, *78*, 1–26. https://doi.org/10.1016/j.jsg.2015.06.006

Rusciadelli, G., Viandante, M. G., Calamita, F., & Cook, A. C. (2005). Burial-exhumation history of the Central Apennines (Italy), from the Foreland to the Chain Building: Thermochronological and Geological data. *Terra Nova*, *17*(6), 560–572. https://doi.org/10.1111/j.1365-3121.2005.00649.x

Rutter, E. H., Hackston, A. J., Yeatman, E., Brodie, K. H., Mecklenburgh, J., & May, S. E. (2013). Reduction of friction on geological faults by weak-phase smearing. *Journal of Structural Geology*, *51*, 52–60. https://doi.org/10.1016/j.jsg.2013.03.008

Scholz, C. (2019). *The mechanics of earthquakes and faulting* (3rd ed.). Cambridge University Press. https://doi.org/10.1017/9781316681473

Scognamiglio, L., Tinti, E., Casarotti, E., Pucci, S., Villani, F., Cocco, M., et al. (2018). Complex fault geometry and rupture dynamics of the M_w 6.5, 30 October 2016, Central Italy Earthquake. *Journal of Geophysical Research: Solid Earth*, *123*(4), 2943–2964. https://doi.org/10.1002/2018JB015603

Sibson, R. H. (1977). Fault rocks and fault mechanisms. *Journal of the Geological Society, London*, *133*(3), 191–213. https://doi.org/10.1144/gsjgs.133.3.0191

Sibson, R. H. (1992). Implications of fault-valve behaviour for rupture nucleation and recurrence. In T. Mikumo, K. Aki, M. Ohnaka, L. J. Ruff, & P. K. P. Spudich (Eds.), *Earthquake source physics and earthquake precursors* (Vol. 211, pp. 283–293).

Siman-Tov, S., Aharonov, E., Boneh, Y., & Reches, Z. E. (2015). Fault mirrors along Carbonate Faults: Formation and destruction during shear experiments. *Earth and Planetary Science Letters*, *430*, 367–376. https://doi.org/10.1016/j.epsl.2015.08.031

Siman-Tov, S., Aharonov, E., Sagy, A., & Emmanuel, S. (2013). Nanograins form carbonate fault mirrors. *Geology*, *41*(6), 703–706. https://doi.org/10.1130/g34087.1

Smeraglia, L., Fabbi, S., Billi, A., Carminati, E., & Cavinato, G. P. (2022). How hydrocarbons move along faults: Evidence form microstructural observations of hydrocarbon-bearing carbonate fault rocks. *Earth and Planetary Science Letters*, *584*, 117454. https://doi.org/10.1016/j.epsl.2022.117454

Smeraglia, L., Mercuri, M., Tavani, S., Pignalosa, A., Kettermann, M., Billi, A., & Carminati, E. (2021). 3D Discrete Fracture Network (DFN) models of damage zone fluid corridors within a reservoir-scale normal fault in carbonates: Multiscale approach using field data and UAV imagery. *Marine and Petroleum Geology*, *126*, 104902. https://doi.org/10.1016/j.marpetgeo.2021.104902

Smith, S. A. F., Billi, A., Di Toro, G., & Spiess, R. (2011). Principal slip zones in limestone: Microstructural characterization and implications for the seismic cycle (Tre Monti fault, Central Apennines, Italy). *Pure and Applied Geophysics*, *168*(12), 2365–2393. https://doi.org/10.1007/s00024-011-0267-5

Smith, S. A. F., Di Toro, G., Kim, S., Ree, J. H., Nielsen, S., Billi, A., & Spiess, R. (2013). Coseismic recrystallization during shallow earthquake slip. *Geology*, *41*(1), 63–66. https://doi.org/10.1130/g33588.1

Spagnuolo, E., Plümper, O., Violay, M., Cavallo, A., & Di Toro, G. (2015). Fast-moving dislocations trigger flash weakening in carbonate-bearing faults during earthquakes. *Scientific Reports*, *5*(1), 16112. https://doi.org/10.1038/srep16112

Speranza, F., Adamoli, L., Maniscalco, R., & Florindo, F. (2003). Genesis and evolution of a curved mountain front: Paleomagnetic and Geological evidence from the Gran Sasso range (Central Apennines, Italy). *Tectonophysics*, *362*(1–4), 183–197. https://doi.org/10.1016/S0040-1951(02)00637-6

Tarasewicz, J. P., Woodcock, N. H., & Dickson, J. A. D. (2005). Carbonate dilation breccias: Examples from the damage zone to the Dent Fault, northwest England. *Geological Society of America Bulletin*, *117*(5–6), 736–745. https://doi.org/10.1130/b25568.1

Tesei, T., Carpenter, B. M., Giorgetti, C., Scuderi, M. M., Sagy, A., Scarlato, P., & Collettini, C. (2017). Friction and scale-dependent deformation processes of large experimental Carbonate faults. *Journal of Structural Geology*, *100*, 12–23. https://doi.org/10.1016/j.jsg.2017.05.008

Tesei, T., Collettini, C., Barchi, M. R., Carpenter, B. M., & Di Stefano, G. (2014). Heterogeneous strength and fault zone complexity of carbonate-bearing thrusts with possible implications for seismicity. *Earth and Planetary Science Letters*, *408*, 307–318. https://doi.org/10.1016/j.epsl.2014.10.021

Toda, S., Lin, J., Meghraoui, M., & Stein, R. S. (2008). 12 May 2008 $M = 7.9$ Wenchuan, China, earthquake calculated to increase failure stress and seismicity rate on three major fault systems. *Geophysical Research Letters*, *35*(17), L17305. https://doi.org/10.1029/2008GL034903

Tozer, R. S. J., Butler, R. W. H., & Corrado, S. (2002). Comparing thin- and thick-skinned thrust tectonic models of the Central Apennines, Italy. In *EGU Stephan Mueller special publication series* (Vol. 1, pp. 181–194).

Trippetta, F., & Geremia, D. (2019). The seismic signature of heavy oil on carbonate reservoir through laboratory experiments and AVA modelling. *Journal of Petroleum Science and Engineering 177*, *177*, 849–860. https://doi.org/10.1016/j.petrol.2019.03.002

Valoroso, L., Chiaraluce, L., & Collettini, C. (2014). Earthquakes and fault zone structure. *Geology*, *42*(4), 343–346. https://doi.org/10.1130/G35071.1

Valoroso, L., Chiaraluce, L., Piccinini, D., Di Stefano, R., Schaff, D., & Waldhauser, F. (2013). Radiography of a normal fault system by 64,000 high-precision earthquake locations: The 2009 L'Aquila (central Italy) case study. *Journal of Geophysical Research: Solid Earth*, *118*(3), 1156–1176. https://doi.org/10.1002/jgrb.50130

Verberne, B. A., Plümper, O., & Spiers, C. J. (2019). Nanocrystalline principal slip zones and their role in controlling crustal fault rheology. *Minerals*, *9*(6), 1–25. https://doi.org/10.3390/min9060328

Verberne, B. A., Spiers, C. J., Niemeijer, A. R., de Bresser, J. H. P., De Winter, D. A. M., & Plümper, O. (2014). Frictional properties and microstructure of Calcite-rich fault Gouges sheared at sub-seismic sliding Velocities. *Pure and Applied Geophysics*, *171*(10), 2617–2640. https://doi.org/10.1007/s00024-013-0760-0

Vezzani, L., Ghisetti, F., & Festa, A. (2010). Geology and tectonic evolution of the Central-southern Apennines, Italy. In *Special paper of the Geological Society of America* (Vol. 469, pp. 1–58). https://doi.org/10.1130/2010.2469

Wibberley, C. A. J., Yielding, G., & Di Toro, G. (2008). Recent advances in the understanding of fault zone internal structure: A review. *Geological Society, London, Special Publications*, *299*(1), 5–33. https://doi.org/10.1144/sp299.2

Won-Young, K., Kulhánek, O., & Meyer, K. (1984). Source processes of the 1981 Gulf of Corinth earthquake sequence from body-wave analysis. *Bulletin of the Seismological Society of America*, *74*(2), 459–477. https://doi.org/10.1785/BSSA0740020459

Woodcock, N. H., Dickson, J. A. D., & Tarasewicz, J. P. T. (2007). Transient permeability and reseal hardening in fault zones: Evidence from dilation Breccia Textures. *Geological Society, London, Special Publications*, *270*(1), 43–53. https://doi.org/10.1144/GSL.SP.2007.270.01.03